3-23-2017

Investigating Analytical and Numerical Methods to Predict Satellite Orbits Using Two-Line Element Sets

Adam T. Rich

INVESTIGATING ANALYTICAL AND NUMERICAL METHODS TO PREDICT SATELLITE ORBITS USING TWO-LINE ELEMENT SETS

THESIS

Adam T. Rich, Captain, USAF

AFIT-ENY-MS-17-M-286

DEPARTMENT OF THE AIR FORCE
AIR UNIVERSITY

AIR FORCE INSTITUTE OF TECHNOLOGY

Wright-Patterson Air Force Base, Ohio

AFIT-ENY-MS-17-M-286

INVESTIGATING ANALYTICAL AND NUMERICAL METHODS TO PREDICT SATELLITE ORBITS USING TWO-LINE ELEMENT SETS

THESIS

Presented to the Faculty

Department of Aeronautics and Astronautics

Graduate School of Engineering and Management

Air Force Institute of Technology

Air University

Air Education and Training Command

In Partial Fulfillment of the Requirements for the

Degree of Master of Science in Astronautical Engineering

Adam T. Rich, B.S.

Captain, USAF

March 2017

AFIT-ENY-MS-17-M-286

INVESTIGATING ANALYTICAL AND NUMERICAL METHODS TO PREDICT SATELLITE ORBITS USING TWO-LINE ELEMENT SETS

Adam T. Rich, B.S.

Captain, USAF

Committee Membership:

William E. Wiesel, Ph.D.
Chair

Lt Col Christopher D. Geisel, Ph.D.
Member

Lt Col Kirk W. Johnson, Ph.D.
Member

Abstract

As Low Earth Orbit (LEO) contains an ever-increasing number of objects, the prediction of future object positions must be precise in order to avoid collisions. Object positions are distributed in two-line element (TLE) sets and are generated using the analytical propagator known as Simplified General Perturbations 4 (SGP4). However, a numerical integrator called Special Perturbations (SP) provides an alternative approach to TLE generation and propagation. In this thesis, TLE accuracy was determined with both models, and the length of time that a single element set can provide valid information was also established. With two-line element sets as data, comparisons were made between the numerical integrator and the analytical model for objects in LEO, particularly the Hubble Space Telescope (HST). The results obtained indicated that the propagated position error using SGP4 remained within 1 km of the expected position during a 7 day period from the epoch of the initial element set. Additionally, the majority of comparisons between SGP4 and SP resulted in a higher error while using the numerical integrator, although some comparisons showed a lower propagated position error with SP. This final result shows a potential for SP to provide more accurate position information than SGP4 in future research.

Acknowledgments

I would like to thank my loving wife for her continued support throughout this long process. Thank you for your encouragement, as it has provided me with a source of inspiration. I would also like to thank my research advisor, Dr. Wiesel. Thank you for your guidance and your dedication to assisting me with this project.

Adam T. Rich

Table of Contents

Page

List of Figures

Page

List of Tables

Page

I. Introduction

As technology has advanced since the dawn of the space age, space assets have had an impact on nearly every conceivable aspect of human life. Imagery, weather, and intelligence gathering satellites permeate Low Earth Orbit, whereas higher orbits contain the majority of navigation and communications payloads. The Global Positioning System (GPS) constellation itself can be considered one of the most widely used space technologies, as GPS receivers function in banking, mining, and utility industries among others, in addition to the myriad of military applications.

With the growing dependence on space assets, precise knowledge of the positions of satellites in space is ever-important. Ground stations require accurate orbit predictions in order to efficiently downlink data from satellite constellations passing overhead, as line of sight to a particular satellite may only last a few minutes per orbit. Military and civilian satellite operators must be constantly aware of the ground trace of their assets in space to effectively complete their mission. Lastly, avoiding a collision, also known as a conjunction, with another object in space is paramount for any space user.

This thesis will investigate two different propagation models used to predict the future positions of objects in space. The North American Aerospace Defense Command (NORAD) generates space object position data in a two-line element set (TLE) format. Most often, the analytical model known as Simplified General Perturbations 4 (SGP4) is utilized to generate and propagate these TLEs. However, an additional numerical integration algorithm, known as Special Perturbations (SP), provides an alternative method for the prediction of future object positions. Using TLEs as data, the propagated positions of objects in Low Earth Orbit (LEO) will be computed, and compared to the

current position provided by updated element sets. With these results, the accuracy of both models will be compared.

1.1 Motivation

Space, particularly in the LEO domain, has become increasingly congested since the first human-made satellite launch of Sputnik 1 on October 4, 1957 [1]. In 1963, the United States Satellite Surveillance Network (SSN) cataloged 616 human-made objects in space. As of 2013, the SSN database of objects in Earth orbit exceeds 23,000 [2]. Of these objects in the catalog, only 5% are operational satellites. The other 95% is comprised of rocket bodies, defunct satellites, and other debris.

Every day, multiple radar and optical sites produce data observations for the SSN. All of this information is then gathered and used by the Joint Space Operations Center (JSpOC), located at Vandenberg Air Force Base, CA, to predict the position of objects in orbit [3]. For a satellite operator, avoiding a collision with another object can be challenging, considering that the probability of collisions between two objects continues to grow as the number of human-made objects in orbit increases.

Ubiquitous in discussions of space situational awareness is the disastrous collision of Iridium 33 and Kosmos 2251 in 2009. Marking the first major collision between two human-made objects in space, this single event produced over 2,000 pieces of debris greater than 10 cm in diameter [4]. Although the Kosmos satellite was defunct at the time of the collision, the multi-million-dollar Iridium 33 was operational. The devastating effect of this event reaches beyond the loss of one satellite. The Iridium-

Kosmos collision effectively disproved the notion that outer space is so large that the likelihood of any two objects colliding is negligible, named the "Big Sky Theory".

Decades prior to this collision, in 1978, Donald Kessler proposed a scenario regarding the large number of objects in LEO. Stating that since the probability of a collision is finite, Kessler argued that one will inevitably occur, producing a large number of debris fragments. That collision would result in a positive-feedback loop of exponentially increasing debris objects and additional collisions [5]. The Kessler Syndrome, as it later became known, described a debris cloud around Earth so massive that it would make LEO as a space domain unusable. With the increasing reliance on space technology in both the military and civilian realms, the result would be disastrous.

1.2 Problem Statement

Satellite operators require more precise knowledge of space objects in orbit. In order to perform avoidance maneuvers, decision makers must be well-informed. Sacrificing fuel to avoid an object would reduce the overall lifespan of that satellite; however, not doing so may result in a collision and therefore the immediate loss of that capability, as well as a debris field that may further impact other payloads. An improvement in the precision of orbit propagation techniques may lead to the avoidance of the scenario proposed by Kessler. Additionally, as perturbation forces continually act on Earth orbiting bodies, even non-propulsive objects have a degree of uncertainty in their orbits. With an increased fidelity in the orbit propagation, a single data point may be able to be relied on for a longer period of time to provide accurate position information on that object. Furthermore, with the continual advancement in computer

processing technology, orbit propagators may now be able to take advantage of numerical integration techniques; these methods may have been previously disadvantageous due to their high computational requirements. Therefore, the viability of incorporating a numerical integrator into the generation of element sets will be investigated in this thesis.

1.3 Research Questions

The focus of this thesis is to further explore orbit propagators in an attempt to determine the accuracy of such systems. NORAD produces data on object positions in space using the Two-Line Element (TLE) set standard, computed with Simplified General Perturbations 4 (SGP4). However, other orbit propagators, particularly the numerical integrator known as Special Perturbations, can also be used. Contrasting the analytical based model with the numerical one, this thesis will seek to address these research questions:

1. What orbit accuracy results can be obtained using TLEs as data with SGP4?
2. Similarly, what accuracy results can be obtained with TLEs using Special Perturbations as the orbit propagator?
3. For what period of time is a single TLE "good"?
4. Does TLE data contain information that can be better used by Special Perturbations?

1.4 Scope

This thesis will investigate the accuracy of orbital positions for objects in Low Earth Orbit. David Vallado has published a MATLAB® version of the SGP4 propagation model [6]. Included in his code is a conversion program between two-line

element sets and position/velocity vectors. Vallado's code provides a method for propagating an Earth orbiting object using SGP4. Additionally, Analytical Graphics Incorporated's Systems Tool Kit (STK) also has SGP4 propagation methods embedded within the program, which can be used to validate the results obtained from Vallado's MATLAB code.

For a numerical integration model, Dr. William Wiesel has developed a program in the C++ language that propagates an object with Special Perturbations using its position/velocity vector [7]. This numerical integration program inputs the start/end epoch times, position/velocity vectors, number of integration steps, and physical Earth properties, and outputs the object's position at each time step through the final epoch time. The output data can then be used in his numerical integration orbit fitting program to obtain a position and velocity vector at the specified epoch time. Finally, position vectors from both Special Perturbations and SGP4 can be compared for various two-line element sets of LEO objects.

II. Literature Review

2.1 A Brief History of Orbit Propagation

In 1957, NORAD was established to provide aerospace warning, aerospace control, and maritime warning in defense of North America. Space situational awareness quickly became a major part of NORAD's mission, as the first human-made satellite was launched later that year. The original development of the series of models known as Simplified General Perturbations (SGP) began in the 1960s and was operational by the early 1970s. In 1980, the propagator source code for SGP4 was released in a document titled *Spacetrack Report #3* [8]. This report documents the entire SGP series equations in full detail, as well as the FORTRAN code for each of the algorithms. For deep space orbits, Simplified Deep Space Perturbations (SDP) models are used as the orbit propagator in lieu of the SGP series. After the release of this document, users requiring accurate position information would apply the SGP and SDP codes to their particular orbit [9]. However, *Spacetrack Report #3* emphasized that the NORAD element sets must only be used with one of the models presented in the report:

> The most important point to be noted is that not just any prediction model will suffice. The NORAD element sets are "mean" values obtained by removing periodic variations in a particular way. In order to obtain good predictions, these periodic variations must be reconstructed (by the prediction model) in exactly the same way they were removed by NORAD. Hence, inputting NORAD element sets into a different model (even though the model may be more accurate or even a numerical integrator) will result in degraded predictions. [9]

2.2 Classical Orbital Elements

The NORAD element sets include parameters that are called the classical orbital elements. For Earth orbiting objects, these six elements are semimajor axis, *a;* eccentricity, *e*; inclination, *i*; right ascension of the ascending node, Ω; argument of perigee, ω; and true anomaly at epoch, T_0 [10].

Semimajor axis describes the size of the orbit and is calculated by adding the perigee and apogee radius and dividing by two. Perigee is the point of closest approach of the orbiting object to Earth, while apogee is the farthest distance from Earth in the orbit. Eccentricity defines the shape of the orbit. An eccentricity of zero describes a circular orbit. As eccentricity approaches a value of one, the orbit becomes more elliptical. A value of exactly one describes a parabolic escape orbit, and an eccentricity greater than one describes a hyperbolic escape orbit. Inclination describes the tilt of the orbit with respect to a reference plane. For Earth orbiting objects, the reference plane is the Earth's equatorial plane [10]. An inclination of 90° indicates a polar orbit.

Right ascension of the ascending node describes the point at which the orbit passes through the equatorial plane while travelling northward. This is measured with respect to a reference direction. The reference direction used is the vernal equinox direction and is defined as the direction of a vector drawn from the Earth to the Sun on the March equinox. The March equinox occurs when the subsolar point crosses the Earth's equator from South to North. Argument of perigee defines the angle between the ascending node and perigee, as measured from the center of the Earth. Finally, true anomaly at epoch defines the angle between the perigee and the position of the object at epoch, also measured from the center of the Earth [10].

Both inertial and non-inertial reference frames are often used with orbit propagation. The Earth Centered Inertial (ECI) reference frame is an example of a non-rotating inertial frame. With an origin at the center of the Earth, this reference frame has a fixed inertial direction that lies along the intersection of the Earth's equatorial plane and the ecliptic plane. Figure 1 is a screenshot taken from STK and depicts an ECI reference frame. In this figure, the inertial direction is the X direction. The Z direction is the Earth's rotation axis direction and is normal to the equatorial plane of the Earth. The Y direction is perpendicular to both the X and Y directions and is also in the equatorial plane of the Earth.

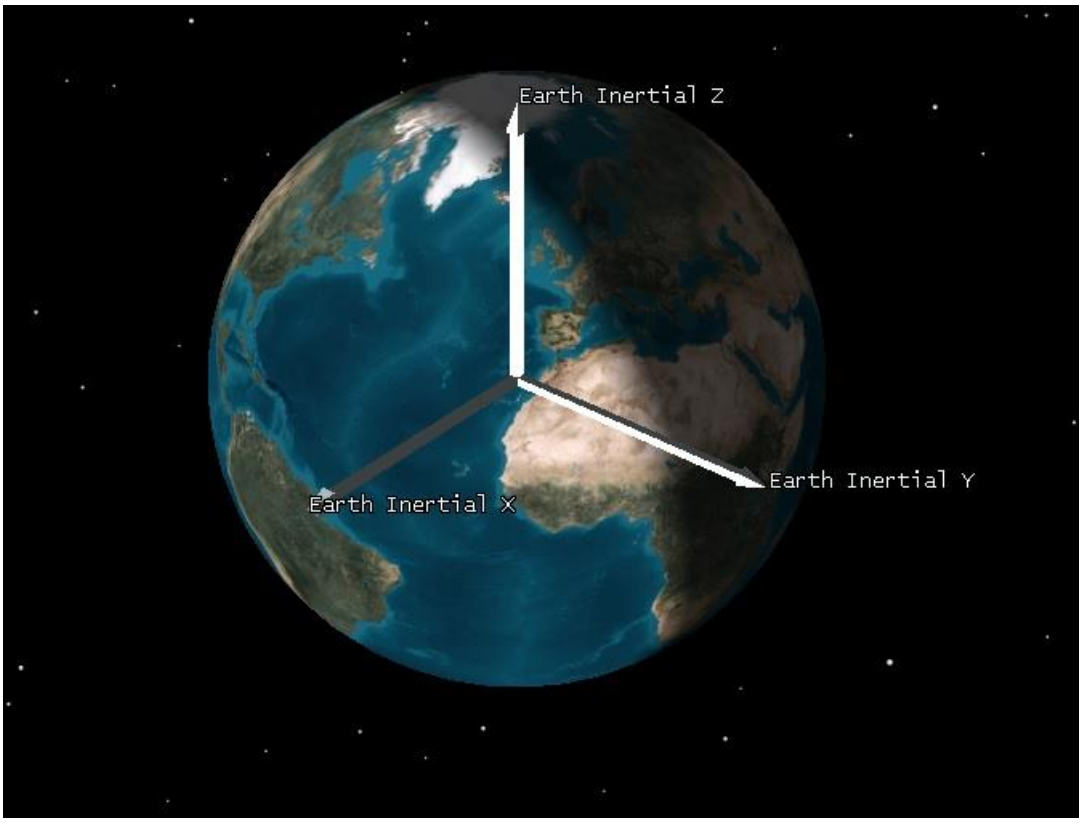

Figure 1: Earth Centered Inertial Reference Frame (STK Screenshot [11])

A commonly used non-inertial reference frame in orbit propagation is the Radial, In-Track, Cross-Track (RIC) reference frame. The principal axis, which is the radial direction, points from the center of the Earth toward the orbiting object. The second axis lies in the orbital plane, is perpendicular to the first axis, and is in the direction of motion of the object. The third axis is normal to the orbital plane, and lies along the angular momentum vector of the orbit [12].

2.3 Two-Line Element Sets

Two-line element sets describe an object's orbit using data from ground-based observation sites. The raw data gathered from the observation sites becomes compiled and converted to an orbit using SGP4. This orbit estimate is then captured in the two-line format. Each TLE contains an epoch time; the object's orbit can be propagated forward or backward in time using the SGP4 model. Figure 2 shows the format of a two-line element set for the NOAA 6 satellite [13]. The first line contains satellite identification information, the current epoch time, as well as the first two time derivatives of mean motion and the object's B-Star drag term. The B-Star coefficient captures the effect of the Earth's atmosphere interacting with the orbiting object. The first two digits of the epoch time refer to the year, the next three refer to the day number, and the decimal refers to the time of day. Classical orbital elements such as right ascension of the ascending node (RAAN), eccentricity, inclination, and argument of perigee appear on the second line. Mean anomaly, mean motion, and revolution number are captured at the end of the second line of the TLE.

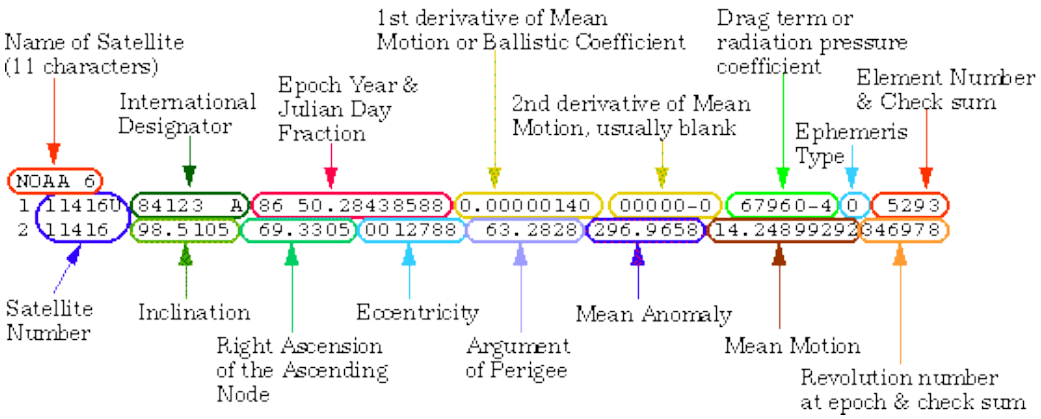

Figure 2: Two-Line Element Set (Reproduced From: NASA [13])

2.4 Orbit Accuracy

As new data reaches the observation sites, NORAD produces a new TLE to update the object's orbit, position, and epoch. NORAD uses the SGP models for producing and propagating the two line element sets. To produce two-line element sets, NORAD employs radar sensors for objects below 6,000 km altitude and electro-optical sensors above 6,000 km altitude [14]. These sensors are positioned throughout the entire Earth to provide global coverage of space objects. Observations from radar sites can include azimuth, elevation, range, and range rate, whereas optical sites can only provide angles (e.g., azimuth and elevation or right ascension and inclination).

In order to update a TLE, observation data must be compared with the expected position of the object as predicted by the previous TLE. The difference between the observed and expected position can then be computed, and the TLE update strives to minimize this difference. Consider one element, x, being the independent variable, with one observation, y, being the dependent variable. Thus, a transformation from element to observation can be given by the function:

$$y = f(x) \tag{1}$$

Letting the actual observation be y_a and the predicted observation be y_p, the derivative of the transformation function at x_p can be given by:

$$\frac{x_a - x_p}{y_a - y_p} = \frac{x_a - x_p}{y_a - f(x_p)} = \frac{dx}{dy} \tag{2}$$

This equation can now be solved for the actual value of the element:

$$x_a = x_p + \left(y_a - f\left(x_p\right)\right) \cdot \frac{dx}{df(x)} \Big|_{x=x_p} \tag{3}$$

This process, known as Newton iteration, can be repeated for each element of the TLE that requires an update. However, in order to perform this iteration, the derivative of the observation with respect to the element must also be computed. A similar approximation method can be used to accomplish this:

$$\frac{df(x)}{dx} = \frac{f(x+\Delta x) - f(x)}{(x+\Delta x) - x} = \frac{f(x+\Delta x) - f(x)}{x} \tag{4}$$

After the process is repeated for each element, the new two-line element set can be produced. T.S. Kelso states that TLEs must be updated when the object's positon exceeds 5 km (within 90% confidence) from the expected position based on the previous TLE [15]. However, TLEs are often updated much more frequently when new data becomes available. For a single TLE, Kelso states that for a LEO, object's position can be expected to remain within 1 km of the predicted position within a few days of the TLE's epoch time [15]. For the purposes of orbit propagation, LEO can be defined as objects having an orbital period of less than 225 minutes [9]

One study, released in 2010 by *Chinese Astronomy and Astrophysics*, conducted research on the accuracy of objects in LEO using SGP4/SDP4 [16]. Orbit positions were computed for two different levels of solar flux, once when the solar 10.7 cm radiation

flow was 100, and again when the value was 200. This study analyzed and calculated the position difference after 1, 3, 7, and 15 days from epoch. The results are displayed in Tables 1 and 2, and show that orbit position error increases with decreasing altitude, and with increasing levels of solar flux. Both results seem intuitive, as the former involves a stronger drag force, and the latter deals with a stronger solar radiation pressure. Increasing magnitude of perturbation forces naturally leads to more uncertainty in the position of an object. Finally, as time from epoch increases, the position error tends to increase in a quadratic fashion.

Table 1: LEO Orbit Prediction Accuracies (F_{10}=100)

Altitude (km)	Test Cases	1 day (km)	3 days (km)	7 days (km)	15 days (km)
$h < 400$	57	4	10	60	300
$400 \leq h \leq 600$	168	3	10	50	100
$600 \leq h \leq 1200$	267	3	10	20	50
$1200 \leq h \leq 7000$	90	2	10	10	20

Table 2: LEO Orbit Prediction Accuracies (F_{10}=200)

Altitude (km)	Test Cases	1 day (km)	3 days (km)	7 days (km)	15 days (km)
$h < 400$	57	10	40	300	1000
$400 \leq h \leq 600$	168	7	30	200	400
$600 \leq h \leq 1200$	267	6	15	70	100
$1200 \leq h \leq 7000$	90	2	10	10	20

A study of two-line element sets was performed by Erin Kahr et al. This analysis involved the use of three LEO satellites with GPS receivers to detect the difference between TLE position information and GPS ephemerides [17]. As a result of their research, Kahr et al. concluded that TLEs can provide position information for LEO objects accurate to within a few kilometers at the time of epoch. Averaging the position difference 15 days from the epoch time of a TLE yielded a predicted vs. actual difference of 50 km. This result was obtained by propagating forward the original TLE to the 15-day TLE and comparing the two position vectors.

Using the RIC reference frame, Kahr et al. noted that the in-track direction contained the most error, an intuitive result considering the majority of a satellite's velocity component is in the in-track direction [17]. The uncertainty contained within the drag estimate of the objects led to the rapid growth of the in-track error. Differences in the radial and cross-track directions were less likely to occur and tended to grow at a slower rate; typically, the former indicates a change in the semimajor axis, while the

latter indicates a change in the inclination. As the radial direction points outward from the satellite (i.e., away from the Earth), an error in that direction requires an error in the measurement of the objects radial distance (i.e., the semimajor axis). Similarly, as the cross-track direction points normal to the orbit plane, a cross-track velocity error indicates an inaccurate measurement of the satellite's inclination. Particularly, significant inclination changes are rare on-orbit, as they involve a perturbing velocity vector normal to the object's direction of motion. As such, the study found that the errors in these two directions were limited to approximately 1 km over the same 15 day period that saw an error of 50 km in the in-track direction.

2.5 Lyapunov Exponents

Although the 2010 study found a quadratic growth in the position error, another discussion point arises given a hypothesis of exponential growth. Lyapunov exponents, named after Russian mathematician Aleksandr Lyapunov, concern such a case. Consider a linearized system that has a solution such that:

$$\delta \dot{\boldsymbol{x}} = A(t)\delta \boldsymbol{x} \tag{5}$$

Given that this system has an initial condition $\delta \boldsymbol{x}(t_0)$, and that the solution grows exponentially, a value, λ, can be defined as:

$$\lambda = \frac{1}{t - t_0} ln \left| \frac{\delta \boldsymbol{x}(t)}{\delta \boldsymbol{x}(t_0)} \right| \tag{6}$$

This expression defines the Lyapunov exponent, and allows for a way to quantify the average rate of exponential growth between time t and t_0 [18]. Furthermore, the multiplicative inverse of the Lyapunov exponent, known as the Lyapunov time, defines

the time interval during which the dependent variable scales by a factor of *e*. For example, consider the function:

$$f(x) = 5e^{4x} \tag{7}$$

For this simple expression, the Lyapunov exponent is 4, and thus the Lyapunov time is ¼. Thus, for every ¼ increment in the independent variable, namely time, the dependent variable scales by a factor of *e*. A short Lyapunov time indicates a rapid exponential growth. For example, if the position error of a satellite's orbit grows exponentially, the error will surpass twenty times its value at epoch in just three Lyapunov time intervals. Conversely, a relatively long Lyapunov time would allow a single TLE to accurately predict an object's position further from epoch.

2.6 Simplified General Perturbations vs. Special Perturbations

As Simplified General Perturbations methods use analytical methods to solve for an approximation to the solution of the equations of motion, they provide for a fast solution and require relatively little computational power. Therefore, SGP4 can provide an orbit's position and velocity vector at a specified future time without needing to calculate each intervening state. However, due to the complexity of the equations of motion of orbital mechanics, higher order terms must be omitted with SGP4. Although SGP4 can be relatively accurate at epoch (as documented in the aforementioned studies), orbit position accuracy degrades as the time from epoch increases.

While SGP4 is widely used by NORAD for generating near-Earth TLEs, other propagation models can also be utilized. Special Perturbations is one such algorithm. SGP4 uses an analytical approach for determining Earth centered satellite orbits, while

Special Perturbations utilizes numerical integration methods [19]. Numerical integration takes into account some of the higher order terms that are omitted with SGP4. Although numerical integration techniques may yield orbit positions accurate to within meters (and therefore more accurate than general perturbations), they require the computation of the object's state vector (to include the position and velocity vector) for each time step increment. As such, propagating an orbit with Special Perturbations involves higher computational power and often a longer time to compute a solution than SGP4 [20]. Additionally, numerical integration methods are only applicable to the specific orbit being integrated; a new integration must be done for each additional orbit that requires propagation.

For further background information, the following references are recommended. Cao, Greene and Montenbruck provide additional information regarding the SGP4 model in their work [21] [22] [23]. Flohrer's research also involves the use of two-line element sets [24].

2.6.1 Atmosphere Models

For its atmosphere modeling, SGP4 uses a simple, static atmosphere model with an assumption of exponential decay [19]. Alternatively, Special Perturbations employs the Jacchia 70 (J70) standard. J70 uses total mass densities derived from orbit analysis and begins at an altitude of 90 km with constant density and temperature. J70 is an empirical model, and as it is constructed from historical data, daily fluctuations are not able to be computed. Thus, Special Perturbations also uses the High Accuracy Satellite Drag Model (HASDM). Derived from tracking observations of approximately 75

calibration objects, HASDM can provide a "nowcast," which can be thought of as a description of present conditions [19]. Special Perturbations can therefore provide a higher level of accuracy in computing the effect of drag, particularly for objects in lower altitudes.

2.6.2 Nongravitational Force Models

The spherical Earth gravitational force term comprises the majority of the force component in the equations of motion for Earth orbiting objects. Although perturbation forces are therefore much smaller (1 part in 1,000) in comparison, they must be carefully considered for accurate orbit propagation. Atmospheric drag and solar radiation pressure are the most prominent nongravitational forces acting on an Earth orbiting satellite. SGP4 incorporates a single ballistic parameter to account for both of these forces, ignoring the inherent physical differences in each. Alternatively, the Special Perturbations algorithm includes parameters that distinguish between drag and solar radiation pressure [19].

Accurately modeling the effects of these nongravitational forces remains particularly challenging. In order to effectively incorporate the higher fidelity atmospheric models into the orbit prediction algorithms, the nongravitational force models must also be sophisticated. Precisely modeling the interaction between the satellite and its environment is a critical part of improving the precision of ephemerides for Earth orbiting satellites [19]. Low Earth Orbit requires a high fidelity drag model; alternatively, in higher orbits (e.g., geosynchronous orbit), the preponderance of the nongravitational perturbation force component is solar radiation pressure. Both

atmospheric drag and solar radiation pressure can vary greatly with solar activity; as such, their magnitudes often fluctuate.

2.6.3 Gravitational Force Models

Among all the forces acting on an Earth orbiting satellite, the gravitational force is the most well-understood, allowing satellite propagators to develop precise gravity models. In addition, both SGP4 and Special Perturbations include perturbation terms within their respective gravity models. Particularly, low-order nonspherical Earth perturbations, as well as solar and lunar third body effects are included in both algorithms. However, as Special Perturbations operates as a numerical integrator, it allows for the use of additional gravitational perturbation terms. Low-order solid and ocean tides, as well as a higher level of geopotential fidelity, are included within the Special Perturbations model [19].

Special Perturbations is likely to see a substantial enhancement with future computational technology. Higher order geopotentials and higher order solid and ocean tides may become available to be integrated into the algorithm. Furthermore, general relativity terms, which can have a non-negligible impact on orbit propagation, could also be included. S. Board et al. believe that these improvements would yield significant improvements to current catalog accuracy [19]. However, general perturbations methods must continue to be studied. SGP and similar analytical methods provide insight into the dynamics of the orbit propagation problem that would be otherwise unattainable by a numerical integrator.

III. Methodology

3.1 Introduction

In an attempt to answer the first research question of Chapter I, "What orbit accuracy results can be obtained using TLEs as data with SGP4," two-line element set data was collected on various objects orbiting in the LEO domain. In order to properly study the accuracy of orbit propagation, non-maneuvering objects must be chosen; intuitively, any propulsive maneuvers performed by the object in question increase the error of future predicted positions.

Incorporating this consideration, the Hubble Space Telescope was chosen to be a primary test subject. As its unique mission set dictates, the Hubble does not have propulsive capabilities and thus is non-maneuvering. Hubble operates in LEO at approximately 540 km in altitude. Since its launch in 1990, the Hubble has been visited numerous times by Space Shuttle missions. Each of these missions involve a rendezvous and docking with the space telescope, which would therefore impart a small but detectable change in the Hubble's orbit. As the last mission to visit the Hubble occurred in 2009, in order to be unaffected by Space Shuttle missions, all TLE data gathered for this research was dated 2010 and later.

Although the Hubble Space Telescope orbits in a relatively high region of the LEO domain, it remains subject to atmospheric drag effects. The effect of drag on the orbiting body is captured in the first line of the TLE in the B-Star term. In aerodynamic

theory, a ballistic coefficient, *B*, is defined as the product of the coefficient of drag, C_D, and the object's cross-sectional area, *A*, divided by its mass, *m* [25]:

$$B = \frac{C_D A}{m} \tag{8}$$

This term represents the level of susceptibility of an object to atmospheric drag effects. To obtain B-Star, the *B* value is multiplied by a reference density, ρ_0, and divided by 2:

$$B^* = B\frac{\rho_0}{2} \tag{9}$$

Therefore, the B-Star term has units of inverse length and is typically measured in inverse Earth radii to obtain more reasonable values. In the TLE, B-Star includes an exponent power to indicate the order of magnitude. For example, if the value indicated in the TLE as "12489-4", this would indicate a value of 0.12489×10^{-4}, or 1.2489×10^{-5}. Lee's research provides more infromation on estimation of the SGP4 drag term [26].

Upon collecting all TLE data for the Hubble for 2010, a Figure 3 was produced showing the various values of the B-Star data contained within the element sets.

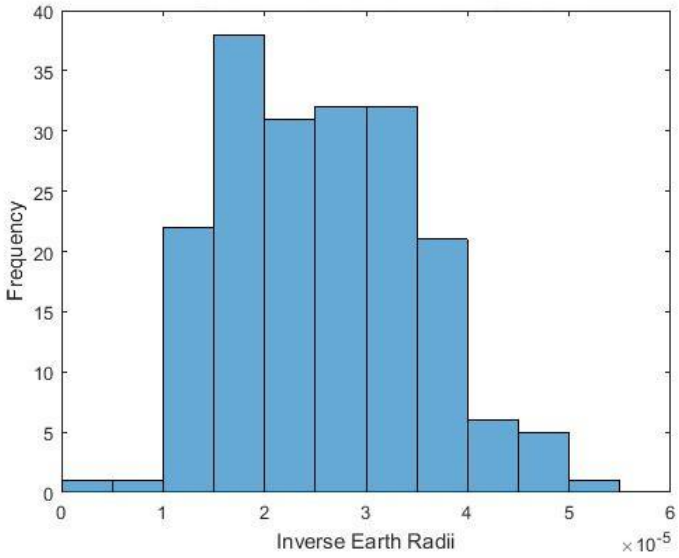

Figure 3: Hubble B-Star Values, 2010

Figure 3 shows a near Gaussian distribution of B-Star values for the Hubble Space Telescope during 2010. The mean value was 2.5816e-05, and the standard deviation was relatively small at 9.4545e-06. In general, as the altitude of an object decreases, the interaction between the object and the atmosphere increases. Although many perturbing forces act on satellites, an object with a lower B-Star may produce more accurate position estimates, as it has less of a disturbing drag force. Due to constantly changing air densities in the upper region of Earth's atmosphere, drag forces acting on satellite remain difficult to model.

3.2 SGP4 Modeling

Two-line element set data was collected on the Hubble Space Telescope for the years 2010 through 2015. For the purposes of this research, the current TLE at epoch is assumed to be the most accurate representation of the satellite's current position. The most updated TLE contains all of the current position information from the ground tracking stations and is therefore used as a baseline for comparison. Additionally, an ECI reference frame was used for all position vector comparisons between SGP4 and Special Perturbations.

The SGP4 modeling involved the use of Dr. Vallado's MATLAB code. First, the TLE data was captured in a text file. From this, his MATLAB program was used to convert each of the two-line element sets into a position and velocity vector. Next, Vallado's MATLAB file titled simply "SGP4" contained code that provided a straightforward method of propagating a position and velocity vector forward in time using the Simplified General Perturbations model.

To determine the accuracy of the SGP4 model using two-line element sets as data, all of the TLE information on the Hubble Space Telescope was gathered and entered into MATLAB. Next, original MATLAB code was written for several test cases to compare an initial TLE and SGP4 propagation with a future TLE position. With this comparison, it was therefore possible to determine the level of accuracy of an initial element set as time progressed away from that epoch time.

Test case 1 involved using the first TLE of that year, which was dated 3 January 2010. Vallado's "SGP4" program allows for the user to input a number of minutes (either forward or backward) away from the TLE epoch time to determine the desired state of the object. Thus, the first two-line element set (TLE 1) was propagated forward in time in this manner. In this way, one could easily determine the number of minutes between TLE 1 and the second element set (TLE 2), input that into the program, and compare the states of both element sets.

Although this is a valid method of comparison, a point-to-point comparison yields only one data point. To obtain a more accurate result with only two element sets, an average over many points in time must be taken. Therefore, a MATLAB program was created that computed the time between each successive element set and then divided that time by 100. Thus, the state for TLE 1 was computed 100 times for the first TLE as time progressed toward the epoch of TLE 2.

In order to obtain accurate comparison results for two different element sets, their positions must be calculated and compared at the same point in time. Thus, as the position states for TLE 1 were computed for each successive increment moving forward, the position state for TLE 2 was also computed. However, the initial time (in minutes)

input into the program for the TLE 2 position was the negative of the epoch time difference. Then, the position states were calculated for TLE 2 in each increment in a similar fashion. Creating the MATLAB script in this manner allowed for each of the two element sets to have position states generated at the same points in time. In this way, TLE 1 was compared 100 times to TLE 2 in the points between their epoch times. Continuing in this fashion, position states for TLE 3 were calculated 100 times for the points between the epoch times of TLEs 2 and 3; these states were also compared to the propagation of TLE 1 to those same points in time. This process was repeated to allow the first TLE to be compared to all of the other element sets of the year 2010 for the Hubble Space Telescope.

After determining the position state for each TLE at each point, the difference of their position was calculated. As each comparison between TLE 1 and a future TLE would yield 200 position states, a method of comparison was needed. For this purpose, the root mean square (RMS) calculation was utilized. Root mean square is, as its name implies, the square root of the arithmetic mean of the square of the values in question. It can be expressed as an equation as:

$$x_{rms} = \sqrt{\frac{1}{n}(x_1^2 + x_2^2 + \cdots + x_n^2)} \tag{10}$$

The term on the left side of the equation is the single RMS value, *n* is the number of terms of the function, and x_1 through x_n are the function terms themselves. Performing the position state comparison in this way allowed for a single value to be generated that essentially acts as an average over 100 data points.

MATLAB contains a function simply called “RMS” that performs the above computation, and this function was used after taking the difference of the two position vectors. Each of the position vectors (corresponding to TLE 1 and the future TLE) contained 100 rows and 3 columns. The result was therefore a vector of 3 indices that represented the average difference for each axis between the two element sets. A single value was desired to illustrate the magnitude of the position difference between TLE 1 and the future element set. Thus, the norm of the 3-D vector was taken. In other words, the indices of the vector were squared, summed, and square rooted to obtain a single value. Repeating this process for each TLE allowed for a method to show the position error growth of the SGP4 propagation of TLE 1 as time grew further way from its epoch. Although predicting the position of a satellite a year may not provide actionable information to decision makers, it remains nevertheless beneficial to determine how quickly the position error increases. For more practical purposes, the comparisons during the first 10 days provide insightful data.

Similarly, other test cases were generated using the same procedure as above. For the 2010 data, test case 2 involved the use of TLE 2 as the initial two-line element set, dated 6 January 2010. TLE 2 was propagated forward in time in the same manner, and its position states were compared against each successive TLE in that year. Furthermore, test cases 3 through 5 follow a similar process, using TLEs 3 through 5 as the initial element set, respectively.

Repeating the process enabled the use of multiple element sets as starting points for position comparisons. As each element set contains updated information from ground based tracking stations, TLEs can vary in their position and velocity precision. These

inconsistencies arise from the slight variability in the accuracy of the data collected. To put that in perspective, a one centimeter per second error in the velocity estimate of an orbiting object will produce a position error of 6 km over the time span of only a week. Thus, using multiple element sets serves to eliminate the variability in the TLE data.

For additional comparisons, TLE data for the Hubble Space Telescope was also procured for the years 2011 through 2015. Test cases 6 through 10 involve the use of the first TLE of each of those years (i.e., test case 6 corresponds to 2011 data, etc.). Again, these element sets were modeled with the SGP4 MATLAB program, and position states compared for each of those years. Taking multiple element sets served to illustrate the differences in the position error growth from year to year. Thus, it remained possible to determine if the most recent element sets produced the lowest future position error.

Additionally, STK models were also generated using SGP4 propagation. Although all the data analysis was based on the MATLAB calculations, STK illustrates and validates the MATLAB results. For example, during test case 1, the position difference between the propagated position of TLE 1 and TLE 50 of 2010 using the SGP4 model yielded a position error of 682 km. Propagating with SGP4 in STK also yielded the same error (to within three significant digits), as shown below in the upper left corner next to the "Range (km)" heading in Figure 4. The blue object illustrates the predicted position of TLE 1, whereas the red object shows the current position of TLE 50 at epoch. Intuitively, the preponderance of the position error is in the in-track direction.

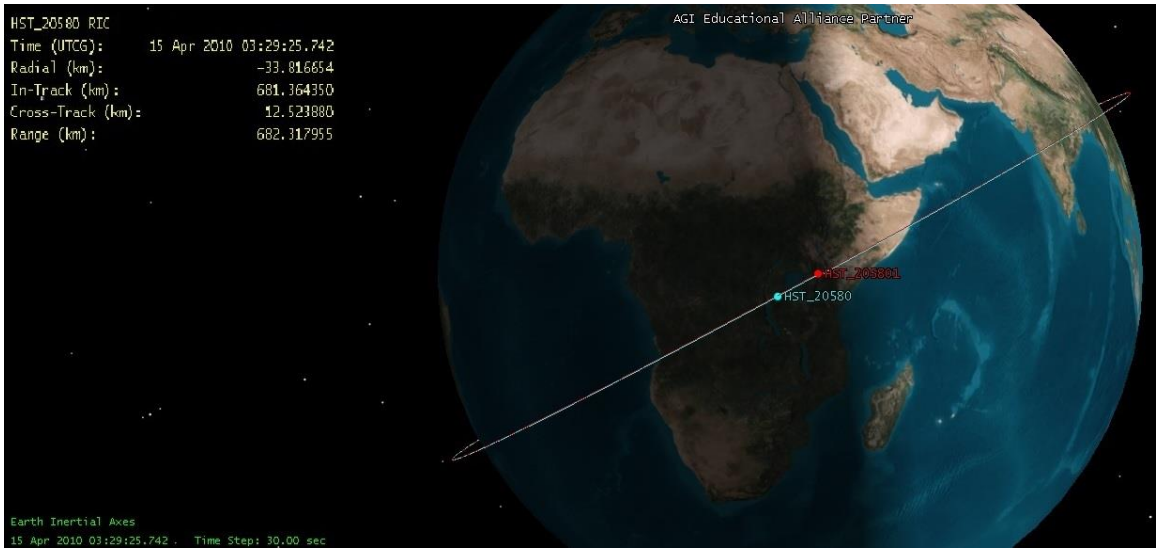

Figure 4: STK Model for Test Case 1 (STK Screenshot [11])

3.3 Special Perturbations

To answer the additional research questions, results were obtained using Special Perturbations as the propagator for element sets. For comparison, the same element sets of the Hubble Space Telescope used in the SGP4 modeling were also used with Special Perturbations. The purpose of performing the analysis in this way was to determine if using two-line element sets as data for use with Special Perturbations produced more accurate results than SGP4, as described in the fourth research question in Chapter I.

Wiesel has authored two C programs, titled "MyTruth" and "Least Squares" that predict future states of an object using the Special Perturbations model [7]. Both programs can be used with or without drag modeling. The "MyTruth" program inputs a geopotential file, the object's initial position and velocity state vectors, as well as the starting and ending times for propagation. The number of outputs and calculation steps

between each output may also be specified. This program then outputs the position state at each time step specified, up through the final time. To obtain accurate results with this program, several hundred calculation steps were used for each test case. As Special Perturbations is inherently a numerical integrator, smaller time steps would generally yield more precise calculations, up to a saturation point.

After running the "MyTruth" program, the data file output containing the position states was then input into "Least Squares." Where the former is essentially an orbit propagator, the latter is an orbit fitting tool. "Least Squares" also inputs the same geopotential file as well as user-defined parameters including the maximum number of iterations to be run and the maximum value for acceptable residual values. Also, an additional file with an estimate of the object's initial position and velocity is a required input.

"Least Squares," as the name implies, takes the position information and attempts to fit a precise orbit using a least squares iteration method. After each attempt, residuals are calculated and the results are used in the successive iteration. An example of a run of this program is shown below in Figure 5.

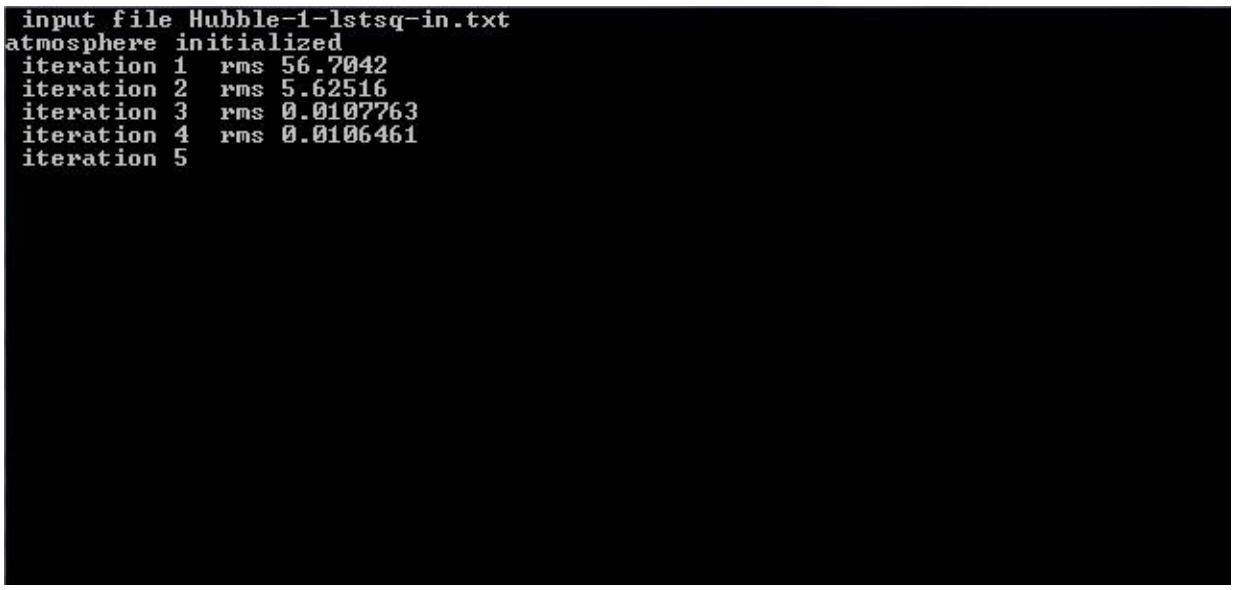

Figure 5: Least Squares C Program Screenshot [7]

This program attempts to reduce the residual RMS values to an acceptable level before finalizing the output. As shown above, the residuals decrease with each successful iteration. Additionally, the program interface displays whether or not an atmosphere model was used. Outputs from "Least Squares" are the initial and final states of the object, to include both its position and velocity vectors.

The same element set data from the Hubble Space Telescope used in test case 1 was also input into the "MyTruth" program for test case 11. Similarly, data from test cases 2 through 9 were also used for test cases 12 through 19, respectively. For the first Special Perturbations test case, TLE 1 from 2010 was input into the "MyTruth" integrator and propagated until the epoch time of TLE 2. For comparison, the position states at each successive TLE were calculated based on the element set at that time. These positions, generated earlier by Vallado's element set to position/velocity state conversion program, acted as the truth model for the Special Perturbations data. In this way, the first

TLE was propagated and its position state compared point-to-point with the next 10 element sets. Choosing 10 future element sets allowed for approximately two weeks of element set data to be captured for each test case.

Additionally, the data file output from the "MyTruth" program was entered into the "Least Squares" orbit fitter. By running the latter program and making an additional comparison, results would indicate if the orbit fitting tool made effective use of the position data. As the orbit fitting tool also produces a position estimate at the final time, this data was therefore able to be compared to the truth model in addition to the original Special Perturbations estimate. Thus, each test case 11 through 20 contained both the "MyTruth" and the "Least Squares" estimate for the first ten element sets beyond the initial TLE. As the initial conditions for Special Perturbations were obtained from the SGP4 element sets, Special Perturbations is expected to have a higher propagated position error than SGP4.

3.4 Additional LEO Objects

Although the Hubble Space Telescope provided for an interesting non-maneuvering test subject for orbital propagation, further test cases were desired. As with the Hubble, these objects must also be non-propulsive. Particularly, lower altitude objects provided for an opportunity to determine the correlation, if any, between altitude (and thus, drag force) and position error. Thus, four additional objects were chosen for this purpose.

Test case 21 focused on a piece of debris from a Delta IV launch vehicle. TLE data was collected from 2010 for this object. At that time, this object held an orbital

altitude of approximately 500 km, slightly lower than that of the Hubble. For this test case, both SGP4 and Special Perturbations were used as orbit propagators. The latter involved the use of both the "MyTruth" and "Least Squares" programs; thus, three different position states were generated and compared to the truth model of the current TLE at epoch. The first element set obtained was dated 1 August 2010 and was propagated forward using both models through the next ten element sets. Continuing with the same process used previously, position states were generated for each TLE with both propagation models and compared to each of the successive element sets.

Similarly, test case 22 concerned a rocket body from a Long March CZ-4B launch vehicle. With a perigee altitude of 562 km, this debris orbited slightly higher than the Hubble Space Telescope during the data taken from 2016. An initial element set in August of that year was propagated forward for ten more element sets using the aforementioned process.

An Indian launched Polar Satellite Launch Vehicle rocket body was the focus of test case 23. Using TLE data from 2016, the process was again repeated. The first element set, dated 1 January 2016, was propagated and compared with the next ten TLE positions. Again, both SGP4 and Special Perturbations models provided position comparison results, yielding three different position state results for each element set.

Finally, an additional Long March rocket body was studied for test case 24. This CZ-6 variant had a perigee altitude of 405 km, making it the lowest object tested for this research. Element sets were taken from 2010, with an initial TLE of 2 January of that year. Performing the same process yielded SGP4 and Special Perturbations comparison results.

3.5 Alternative Model

One final test case involves an alternative approach to obtaining the initial conditions for Special Perturbations. Test case 25 used TLE data from test case 12 for the Hubble Space Telescope. The SGP4 position error was calculated in the same way as done previously. However, the initial position and velocity vector for the Special Perturbations model was obtained in the following manner.

The MATLAB SGP4 program was used to propagate several thousand position states for the Hubble for a one day period. This data set was then entered into the "Least Squares" orbit fitting program. The outputs of that program were initial position and velocity vectors that differed from the original state vectors computed by SGP4. With the new initial conditions, the "MyTruth" program was used to propagate forward the future positions of the Hubble. Finally, the new Special Perturbations data was compared with the SGP4 data for the next ten element sets.

IV. Results

4.1 Test Case 1

Figure 6 below illustrates the position error growth for the Hubble Space Telescope using 2010 data. The first element set, dated 3 January, was propagated forward in time and compared to the remaining element sets of that year. These results were obtained by taking 100 data points between each element set, using the root mean square function, and then taking the square root of the sum of the squares of each of the three indices in the position vector.

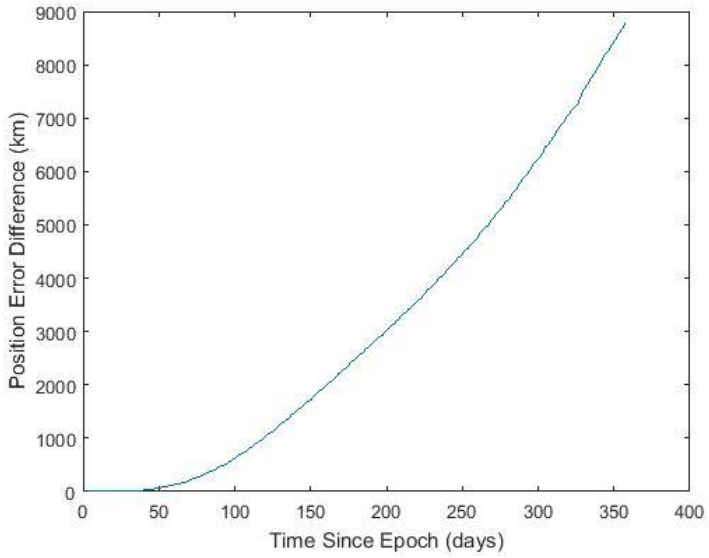

Figure 6: Test Case 1, Propagated Position Error vs. Time (2010 Data)

As can be seen from the figure, the position error grew in what appears to be a quadratic fashion. Thus, fitting a second order polynomial curve fit to the data produced an extremely close match. Using the basic curve fit tool provided by MATLAB, Figure 7 was obtained.

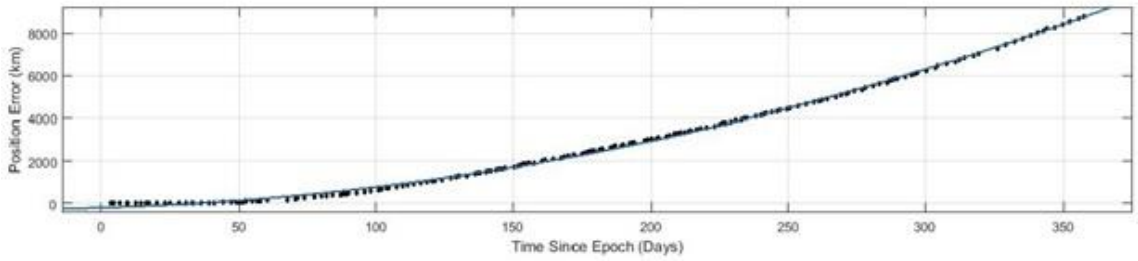

Figure 7: Quadratic Curve Fit

The curve fit resulted in a nearly identical match, with an R-squared value of 0.9988. To clearly show the data for the first 50 days since epoch, an additional graph was generated.

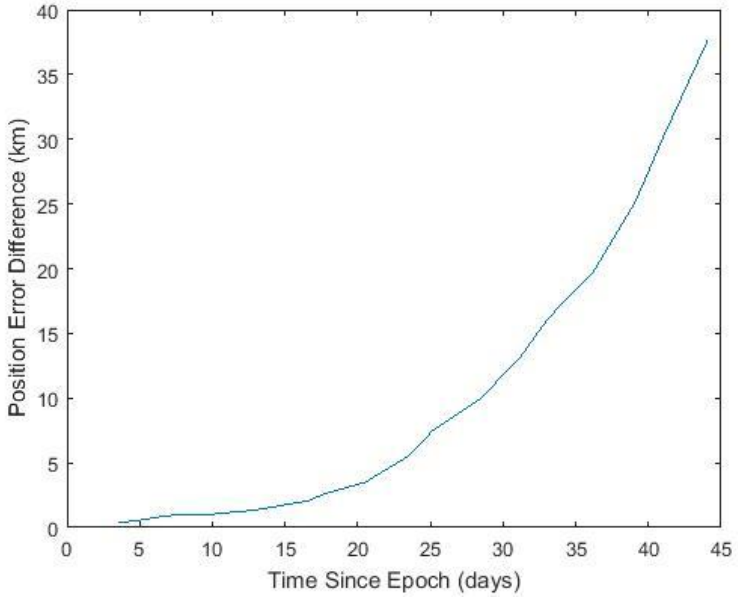

Figure 8: Test Case 1, Short Term Propagated Position Error vs. Time (2010 Data)

Figure 8 indicates that the average position error of the Hubble Space Telescope based upon the initial element set remained within 1 km of the propagated position through the first 9 days since epoch. That particular period of time spanned five element sets. As shown in the figure, the error growth began to increase rapidly after that, reaching 30 km within the first 40 days.

4.2 Test Case 2

Test case 2 produced similar results using the second element set from 2010, dated 6 January, as the initial TLE. These results are displayed in Figure 9, below.

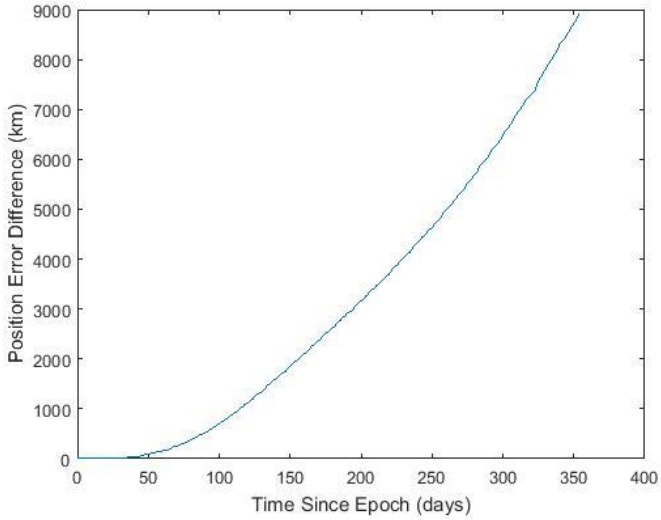

Figure 9: Test Case 2, Propagated Position Error vs. Time (2010 Data)

Additionally, Figure 10 shows the data for the first 50 days since epoch.

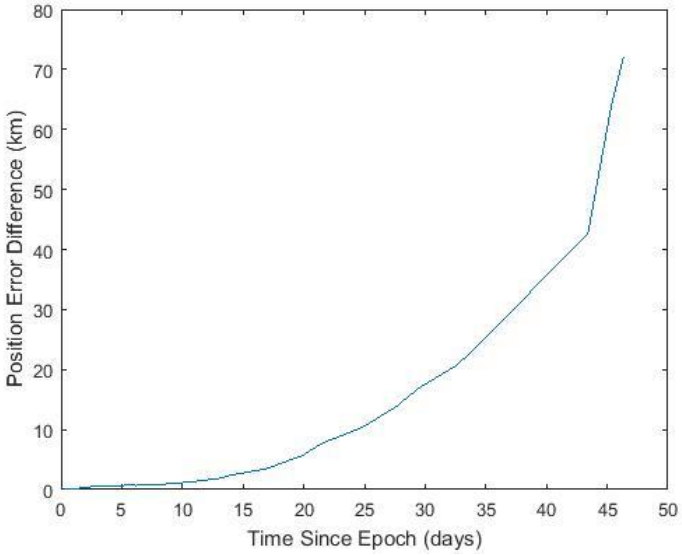

Figure 10: Test Case 2, Short Term Propagated Position Error vs. Time (2010 Data)

These results show that the position error for the second test case remained within 1 km for the first 12 days since epoch. However, the error grew at a much higher rate following the initial slow climb, surpassing 20 km after 33 days, and 50 km after only 45 days. The sharp increase occurring 44 days from epoch is a result of a longer than average time between element sets.

4.3 Test Case 3

Starting with the third element set of 2010, test case 3 yielded results similar to the previous two test cases. The initial TLE was also dated 6 January; however, it occurred in a later part of that day than did the previous initial element set. Figure 11 displays the propagated position errors for this test case.

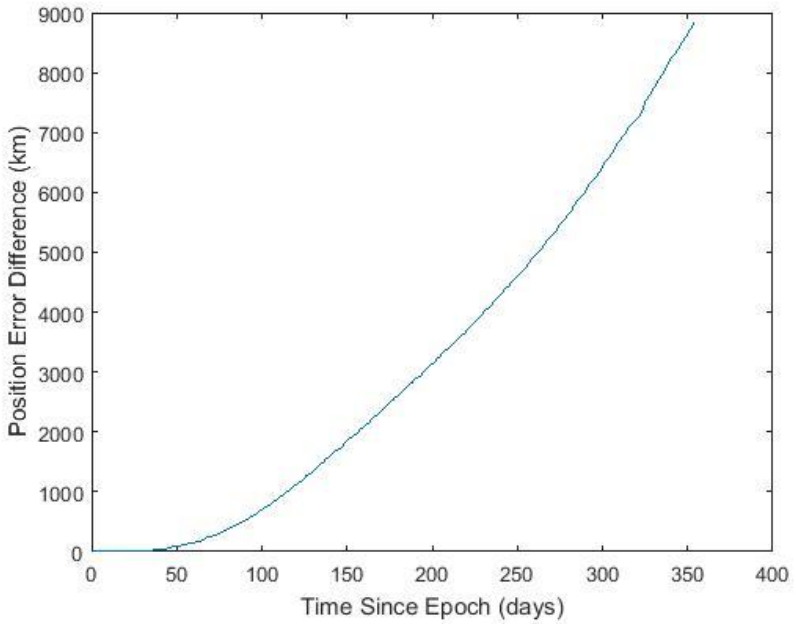

Figure 11: Test Case 3, Propagated Position Error vs. Time (2010 Data)

The data gathered continued to display a quadratic increase in the satellite's position error. Taking closer look at the first 50 days form epoch, Figure 12 illustrates the shorter term propagation. The position error remained within 1 km for 9 days from epoch. As seen in the figure, the propagated position error then rose in a somewhat quadratic manner until rapidly increasing toward the end of the 50 day period.

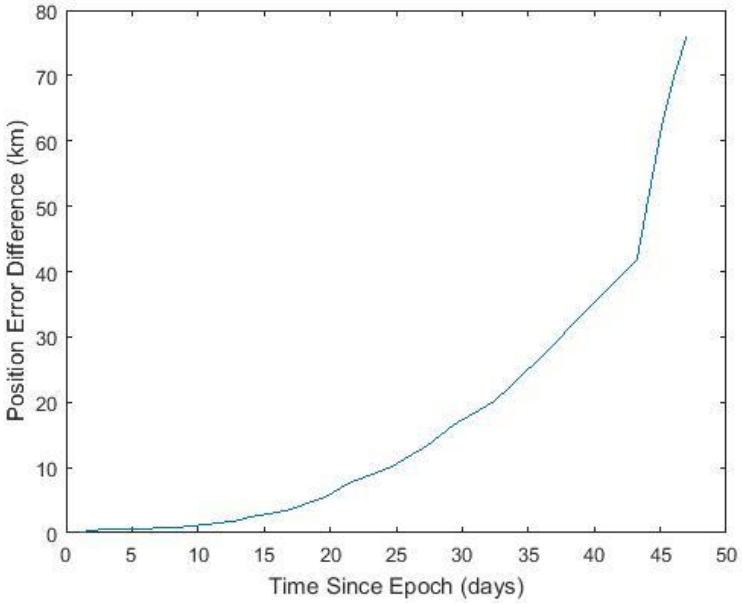

Figure 12: Test Case 3, Short Term Propagated Position Error vs. Time (2010 Data)

4.4 Test Case 4

Following the same procedure as the previous test cases, test case 4 began with an initial element set dated 7 January. Propagating this TLE through the remaining element sets of 2010 yielded the results shown in Figure 13.

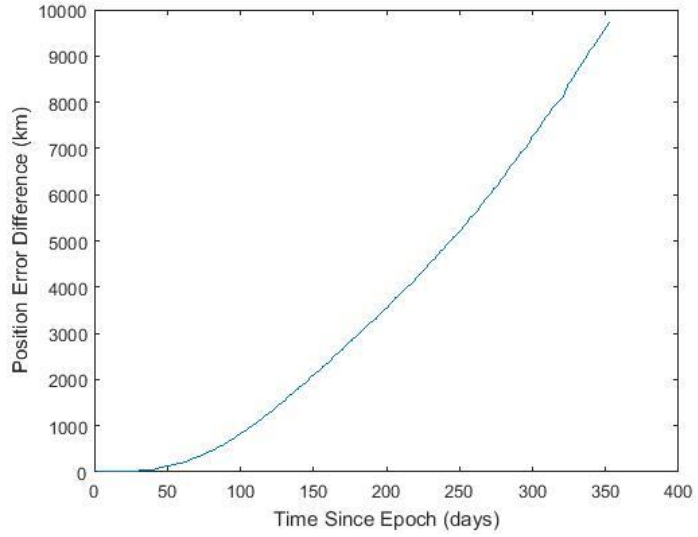

Figure 13: Test Case 4, Propagated Position Error vs. Time (2010 Data)

Although rising in the same quadratic fashion, this test case showed a more rapid increase in the position error growth than the previous test cases. Focusing on the first 50 days from epoch, Figure 14 shows the short term propagation error.

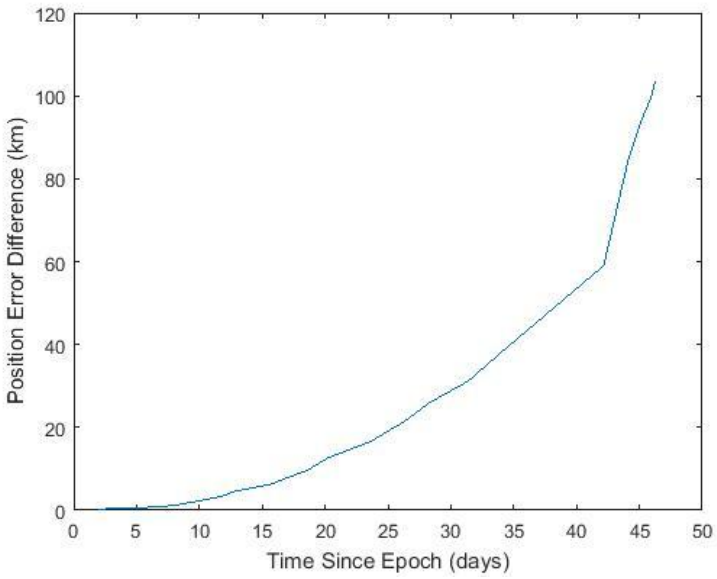

Figure 14: Test Case 4, Short Term Propagated Position Error vs. Time (2010 Data)

The propagated positon remained within 1 km for only 5 days before rapidly increasing. Displayed in the curve above, this test case produced the fastest growing position error yet, as the error surpassed 100 km by the 45 day point. At that point, the propagated position error was increasing at an extremely high, nearly linear rate.

4.5 Test Case 5

The TLE from 9 January, 2010 was the starting point for test case 5. Figure 15 shows the familiar quadratic increase in the position error.

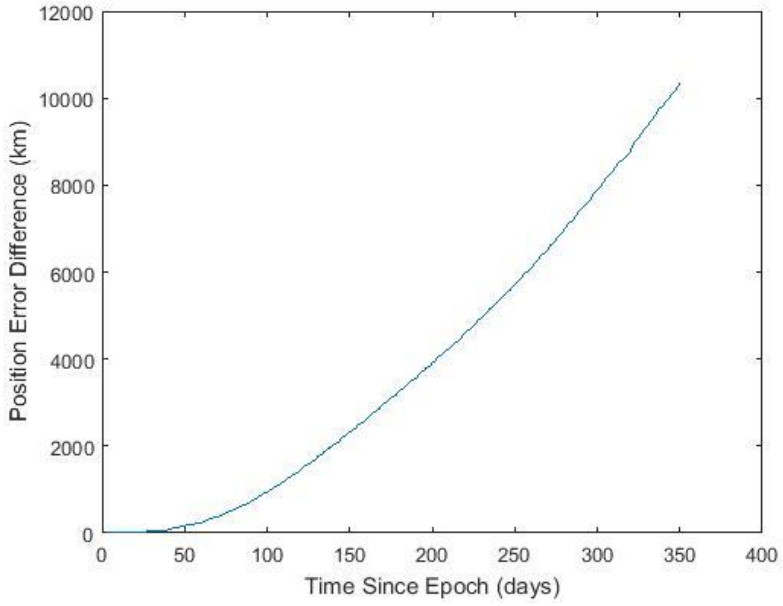

Figure 15: Test Case 5, Propagated Position Error vs. Time (2010 Data)

The results from test case 5 displayed a still higher rate of increase in the error growth. This test case was the first to surpass the 10,000 km position error within the year timeframe. Again, the resulting curve illustrated a quadratic growth in the propagated position error. Figure 16 displays the first 50 days from epoch.

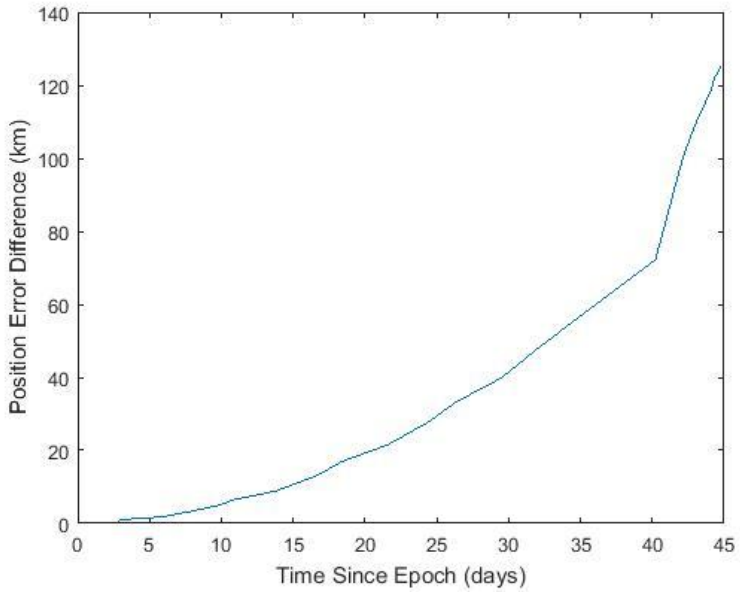

Figure 16: Test Case 5, Short Term Propagated Position Error vs. Time (2010 Data)

Although the position error remained within 1 km for 13 days during this test case, the rapid growth following that initial period surpassed the earlier cases. The propagated position error rose to 120 km by 42 days from epoch.

Despite the fact that all five test cases displayed a quadratic growth in the position error, the results obtained support the hypothesis that TLEs can vary greatly in their orbital element accuracy. Although propagating a satellite's position a year into the future may seem to be an excessively long timescale for predicting satellite orbits from a single element set, more practical data can be obtained from focusing on the first few days from epoch.

4.6 Test Case 6

In order to obtain a variety of data points, test cases 6 through 10 concern the element sets obtained from the years 2011 through 2015, respectively. Figure 17 displays

the results for the year 2011, starting with an initial element set dated 2 January of that year.

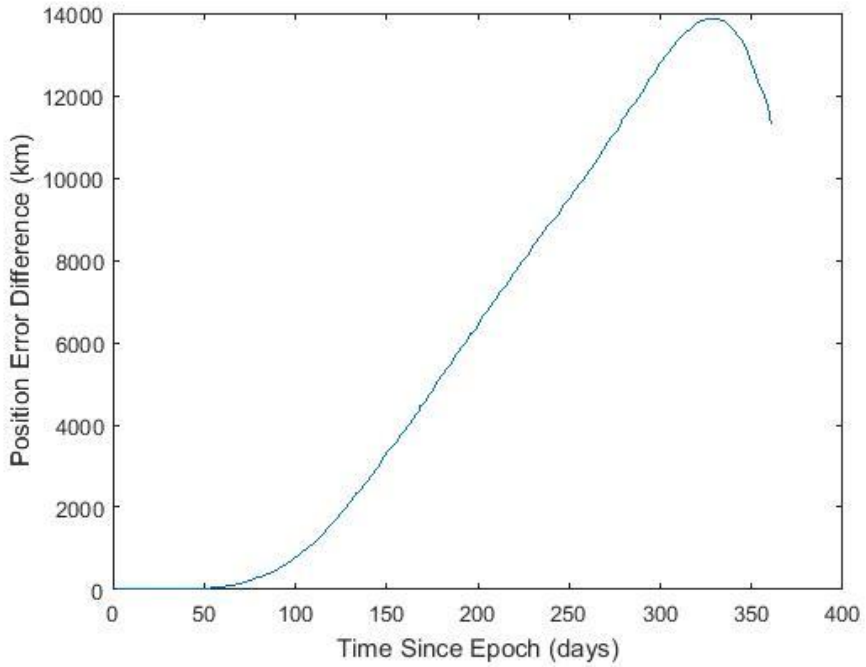

Figure 17: Test Case 6, Propagated Position Error vs. Time (2011 Data)

At first, the results from 2011 show the expected quadratic increase in the error growth. However, as shown above, as the error approaches approximately 14,000 km, the growth rate decreases and eventually reverses. Although unusual at first glance, this is considered an expected result. As the Hubble Space Telescope orbits at an altitude of 540 km, its distance from the center of the Earth is therefore just under 7,000 km. Additionally, the preponderance of the propagated position error is in the in-track direction. As the error grows, it reaches a maximum value equal to twice the distance between the satellite and Earth. At that point, the estimated position is 180° ahead of (or behind) the true position of the object in its orbit. Thus, as the time from epoch increases

beyond that point, the propagated position will start to become closer to the true position again. Therefore, the initial element set from test case 6 must have a lower precision in its orbital elements than the previous test cases. Looking at the first 50 days from epoch, Figure 18 shows the short term results.

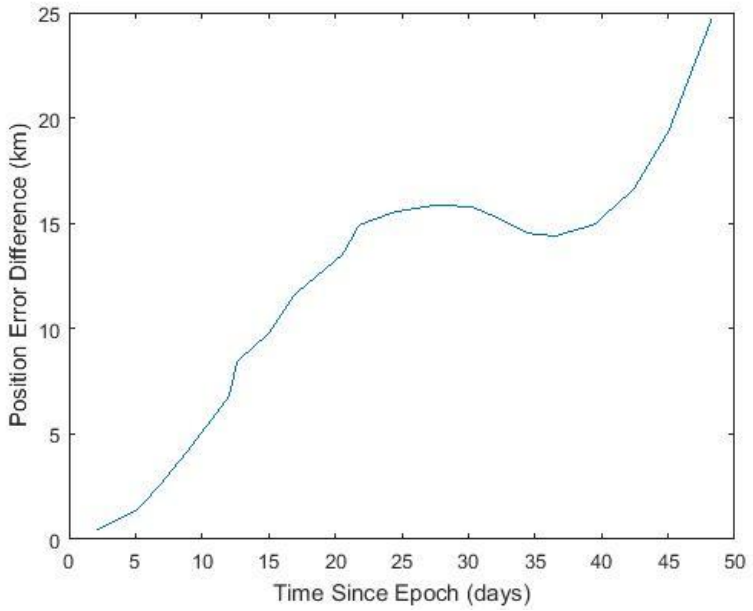

Figure 18: Test Case 6, Short Term Propagated Position Error vs. Time (2011 Data)

At first, the position error grows somewhat quickly, although it remains within 1 km for 12 days. Interestingly, the error actually decreases between days 25 and 35 from epoch. Past this point, however, it quickly rises again in a quadratic fashion.

4.7 Test Case 7

Test case 7 started with an initial TLE of 5 January, 2012. Figure 19 indicates that the position error again grew in a quadratic manner. As the error began to approach the 14,000 km point, its increase began to slow. If additional element sets were obtained, the error would most certainly decrease as it did in test case 6.

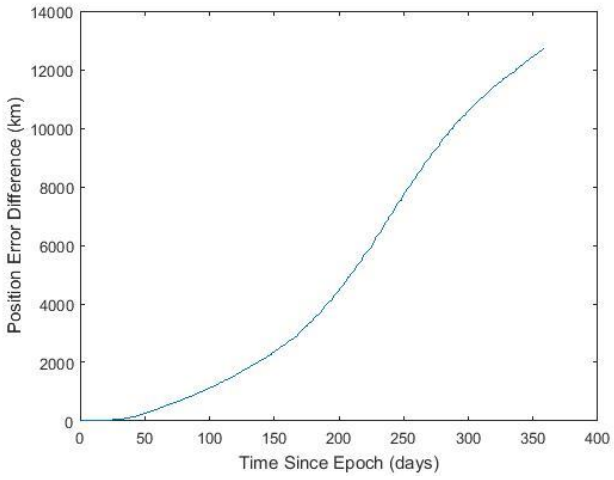

Figure 19: Test Case 7, Propagated Position Error vs. Time (2012 Data)

Displaying the first month since epoch, Figure 20 shows the short term position error. The propagated error remained within 1 km for 4 days then began to rise. After a short decrease in the error (which may have been caused by a single outlier element set), the position error growth quickly resumed the familiar quadratic form.

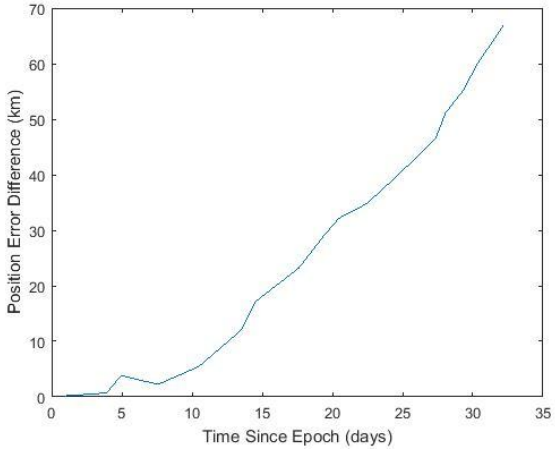

Figure 20: Test Case 7, Short Term Propagated Position Error vs. Time (2012 Data)

4.8 Test Case 8

Test case 8 started with the element set dated 1 January of 2013. As shown below in Figure 21, the position error experienced an initial period of relatively slow growth before rising in a quadratic fashion. Furthermore, the position error did not approach the maximum value as it did in the previous two test cases. This indicates that the initial element set used for propagating the future position contained more accurate information than in the previous cases.

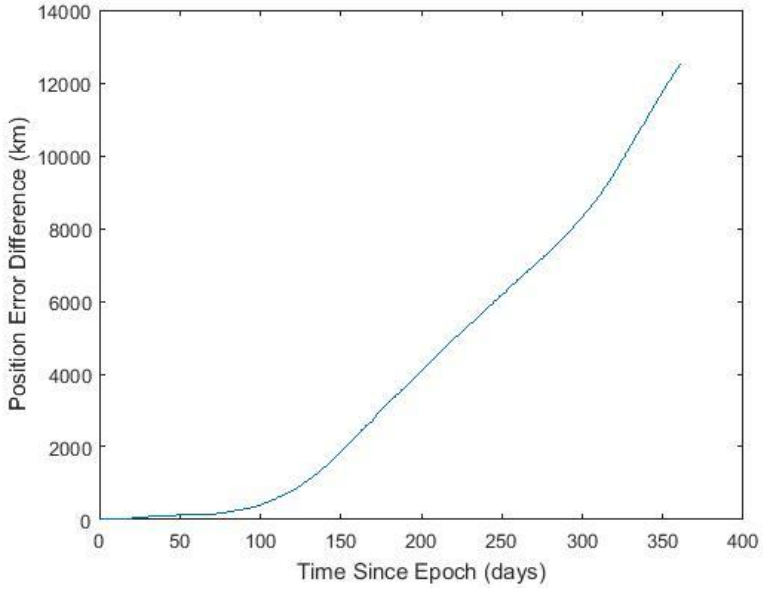

Figure 21: Test Case 8, Propagated Position Error vs. Time (2013 Data)

Focusing on the first month since epoch, the results from Figure 22 show that the positon error of test case 8 initially rose relatively slowly. The propagated position remained within 1 km for 9 days. After that, the error began to increase rapidly and grew to 50 km by the 22nd day from epoch.

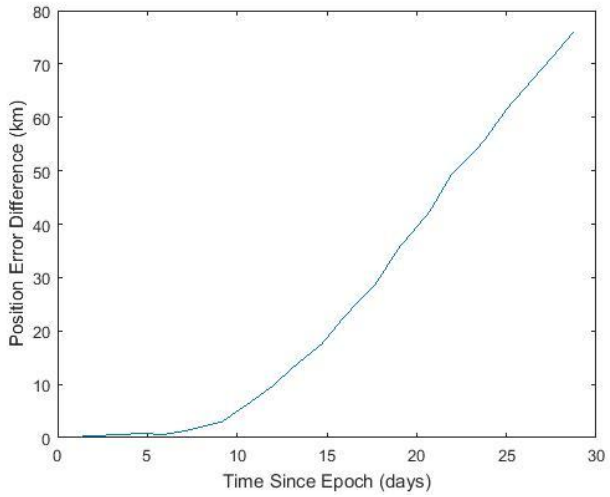

Figure 22: Test Case 8, Short Term Propagated Position Error vs. Time (2013 Data)

4.9 Test Case 9

Starting with a TLE dated 9 January, 2014, test case 9 resulted in the data shown in Figure 23. The position error growth was so rapid, that it increased to the maximum value twice in the time period of a year. This indicates a highly inaccurate data set contained within the initial TLE.

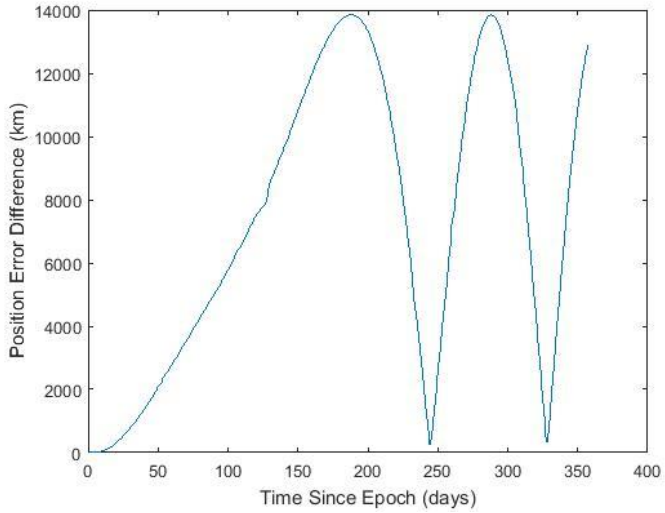

Figure 23: Test Case 9, Propagated Position Error vs. Time (2014 Data)

For the first month, however, the data shows a quadratic growth in the position error. From Figure 24, the position error rose to 100 km after only 12 days. Test case 9 proves to have the highest error growth yet, as the error surpassed 500 km within the first 25 days from epoch.

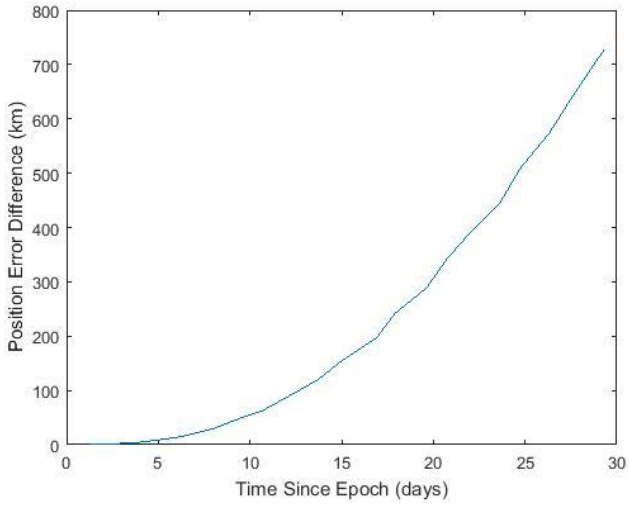

Figure 24: Test Case 9, Short Term Propagated Position Error vs. Time (2014 Data)

4.10 Test Case 10

Test case 10 began with an initial element set of 2 January 2015. As Figure 25 indicates, the results from this case were similar to those found in test case 6. Within one year from epoch, the propagated position error approaches the maximum value and begins to decline after the 250 day point. However, unlike test case 9, the error in the 2015 data does not make full cycles of maximum and minimum error.

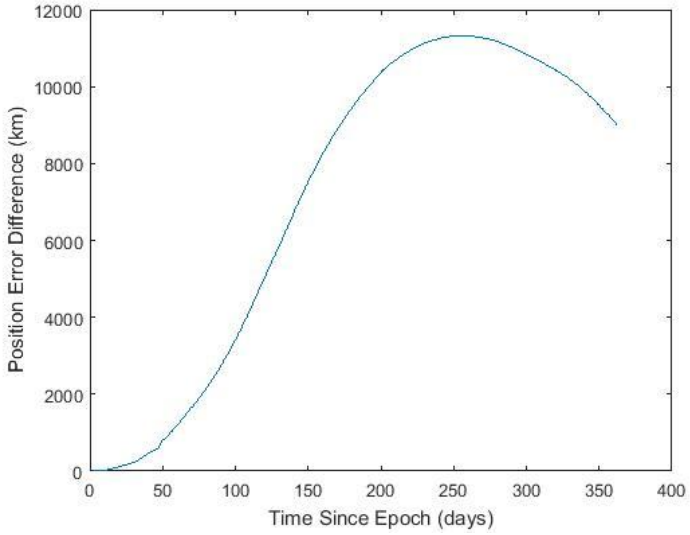

Figure 25: Test Case 10, Propagated Position Error vs. Time (2015 Data)

In the first month since epoch, Figure 26 displays the familiar quadratic rise in the error for the 2015 case. After remaining within 1 km for 6 days, the error begins to rapidly increase, surpassing 100 km by 20 days from epoch.

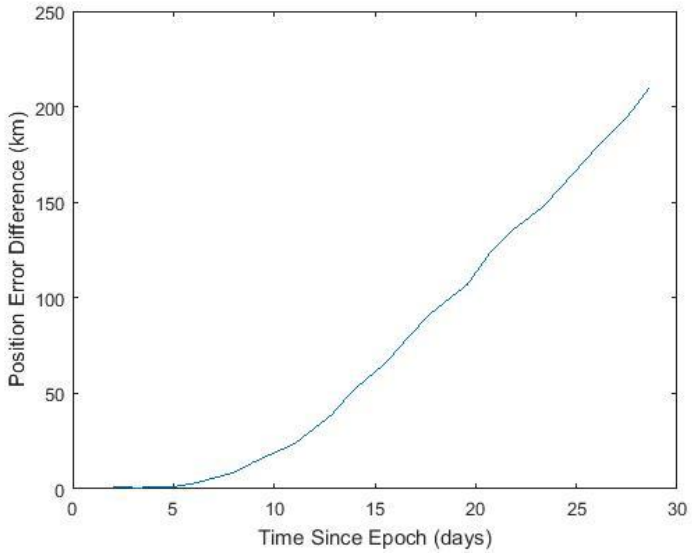

Figure 26: Test Case 10, Short Term Propagated Position Error vs. Time (2015 Data)

Having completed the first ten test cases using SGP4 propagation, a comparison of the data gathered is necessary. Table 3 summarizes the aforementioned results, displaying the time period required for the position error of each test case to surpass 1, 5, and 10 km.

Based on the results displayed in Table 3, the position error from the first three test cases remained close to their respective truth models for the longest period of time. Test cases 2 and 3 were nearly identical, while the first test case showed the best overall results. Alternatively, data taken from later years (particularly 2014) showed the fastest position error growth. In comparison, in the time that the error from test case 9 had surpassed 10 km, the error from the first test case was less than 1 km.

Table 3: SGP4 Propagation Error

Test Case #	Days Until 1 Km Error	Days Until 5 Km Error	Days Until 10 Km Error
1	9.1	22.7	28.5
2	9.2	19.0	24.4
3	9.2	18.9	24.5
4	7.2	13.5	18.8
5	2.9	9.8	14.6
6	3.8	9.9	15.3
7	4.0	10.0	12.6
8	6.6	10.0	12.1
9	1.2	4.1	5.2
10	4.3	6.7	8.2

4.11 Test Case 11

The remaining test cases now involve the comparison of the SGP4 and Special Perturbations models. The TLE data used in the test cases 11 through 20 are identical to those in test cases 1 through 10, respectively. However, instead of using a weighted average of 100 data points per element set pair, the following results displayed are based on point by point comparisons between the two models. This method of data collection was necessary in order to compare the two models at the same epoch times. During each comparison, a verification was made to ensure that the positions were calculated at the same point in time. In all cases, the epoch times for comparisons between the two models differed by a time period on the order of tenths of a second, which is assumed to be negligible.

Test case 11 takes the element sets for the Hubble Space Telescope from 2010 data. Point by point comparisons for SGP4 and Special Perturbations were made between the first element set of that year and the following ten TLEs. Both the "MyTruth" and the "Least Squares" programs were used for the numerical propagation; however, in all tested cases, the results from both programs were essentially identical. In fact, at their greatest difference, the two programs agreed to within 4 significant digits. As such, the following results will only show the data obtained from the "MyTruth" program, as displaying both sets of Special Perturbations data would be redundant. Figure 27 shows the results for test case 11, displaying the propagation position error for both SGP4 and Special Perturbations.

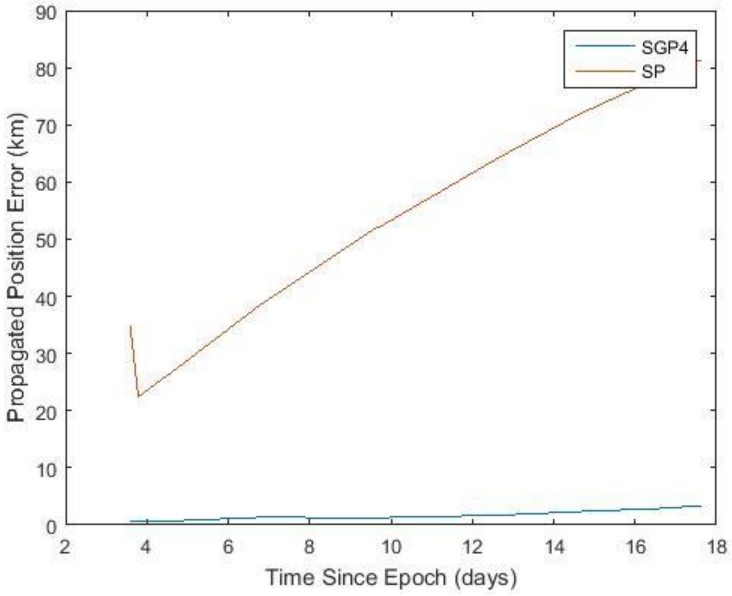

Figure 27: Test Case 11, SGP4 vs. Special Perturbations (2010 Data)

From the figure above, the Special Perturbations model starts at a 35 km difference at 3 days from epoch before dropping to approximately 22 km difference. The first data point appears to be an outlier, based on the steady increase in the error following the second point. Compared to SGP4, the Special Perturbations error grew much more rapidly during the first ten element sets. In fact, compared to Special Perturbations, the SGP4 error growth appears to be almost negligible.

4.12 Test Case 12

Test case 12 involved the use of the second element set of 2010 as the initial propagation point. Figure 28 displays the results of this test case.

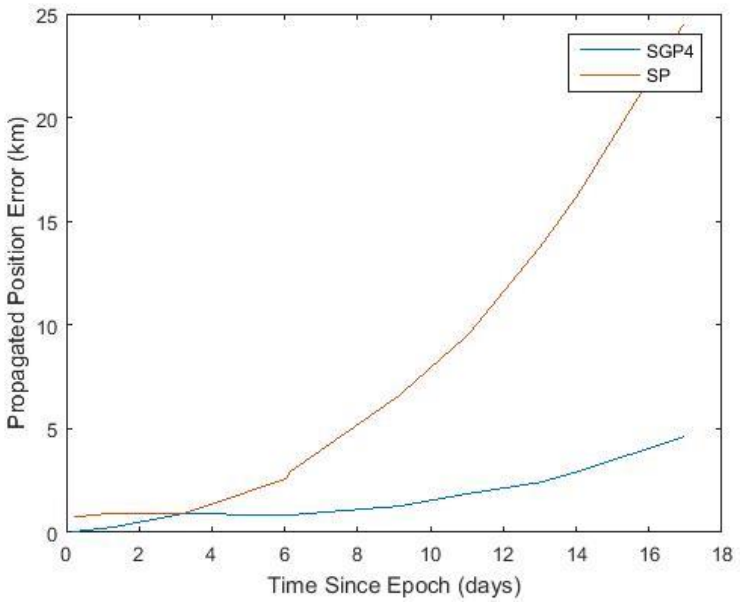

Figure 28: Test Case 12, SGP4 vs. Special Perturbations (2010 Data)

Based on the figure above, the error for the Special Perturbations model grows at a faster rate than its SGP4 counterpart. At the third data point, though, Special Perturbations does have a lower position error than SGP4; however, the difference in their error is only 6 meters and is negligible.

4.13 Test Case 13

In accordance with the same process as in the previous two test cases, the third element set of 2010, dated 6 January, was used to propagate the positions of test case 13. The results are shown in Figure 29.

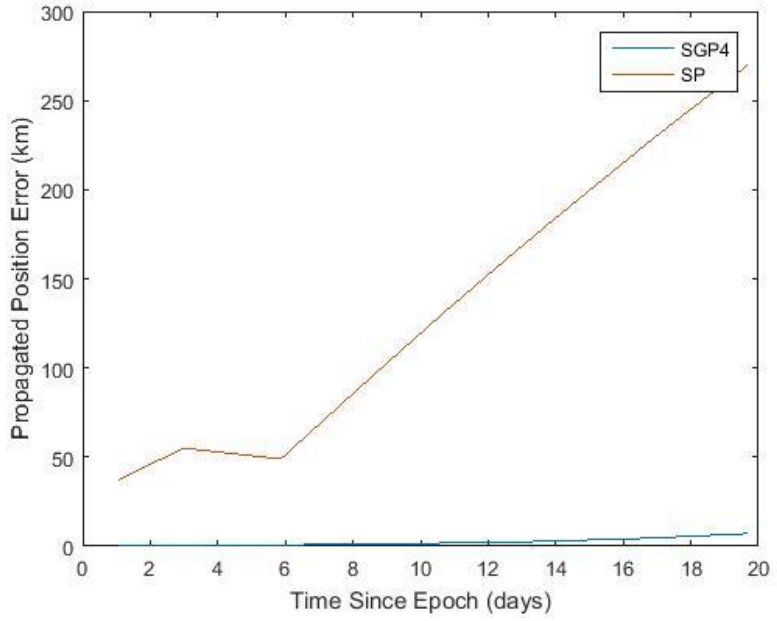

Figure 29: Test Case 13, SGP4 vs. Special Perturbations (2010 Data)

Again, a much higher rate of increase for Special Perturbations is shown. After the first few points, the error for Special Perturbations increases at a constant, linear rate; alternatively, the error for SGP4 remains much lower during this period.

4.14 Test Case 14

Similarly, test case 14 took the fourth TLE from 2010 as its starting point. Again, the results shown a much higher rate of increase in the error for Special Perturbations. After approximately five days from epoch, the propagated position error for Special Perturbations begins to increase at a linear rate. Meanwhile, the propagation error for SGP4 continues to remain at lower values during the first ten element sets.

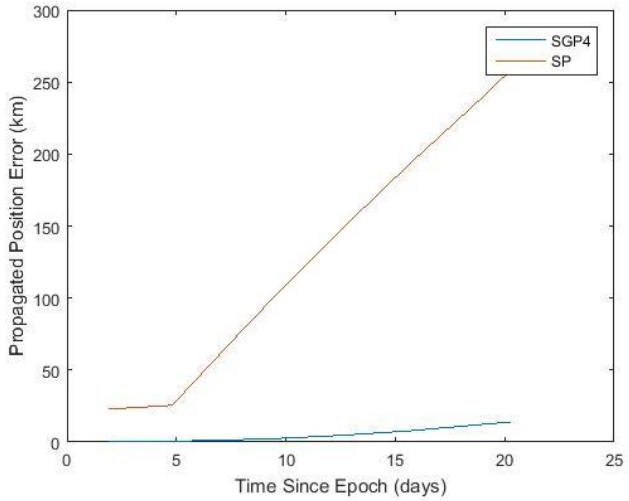

Figure 30: Test Case 14, SGP4 vs. Special Perturbations (2010 Data)

4.15 Test Case 15

Test case 15 was the last case for 2010. Initially, the Special Perturbations error was comparable with the SGP4 error for the first data point. However, as Figure 31 shows, the error increased almost vertically following the second data point and continued a rapid increase. Again, the error using SGP4 increased at a much slower rate.

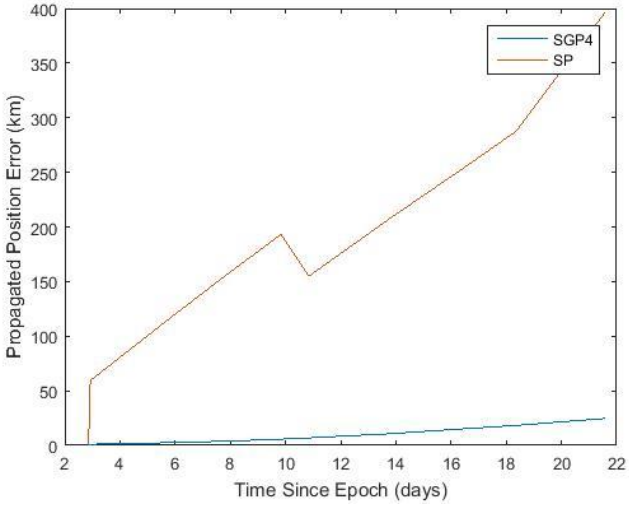

Figure 31: Test Case 15, SGP4 vs. Special Perturbations (2010 Data)

4.16 Test Case 16

Using the first element set of 2011 for the initial propagation, test case 16 continued to show similar results. Figure 32 illustrates a somewhat smoother increase in the error of the Special Perturbations propagation. The error using SGP4 again remained relatively low.

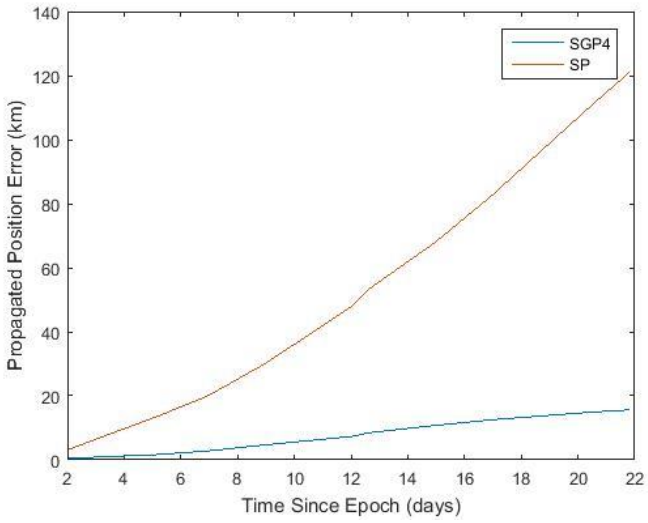

Figure 32: Test Case 16, SGP4 vs. Special Perturbations (2011 Data)

4.17 Test Case 17

Similar results were obtained for test case 17 using a 2012 element set data. Figure 33 shows that the error using Special Perturbations as the propagation method increased so rapidly that it surpassed 600 km within 18 days. Alternatively, the error for SGP4 remained much lower through the same time period.

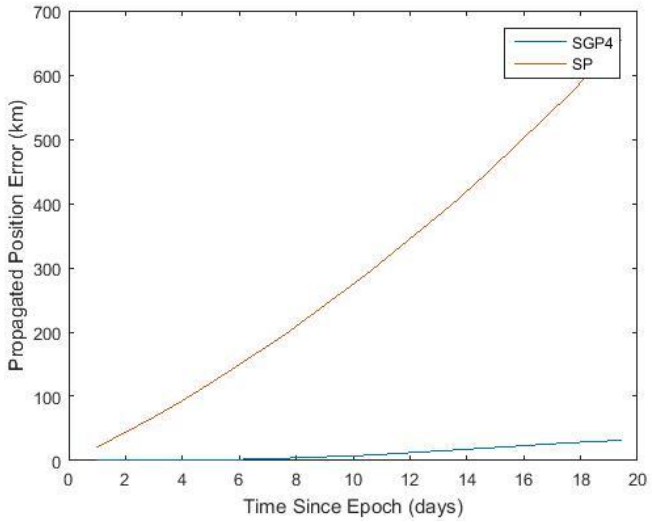

Figure 33: Test Case 17, SGP4 vs. Special Perturbations (2012 Data)

4.18 Test Case 18

For the 2013 test case, the error for Special Perturbations was initially comparable to SGP4. However, after 2 days, the former began to grow in quadratic fashion, while the latter increased at a much slower rate.

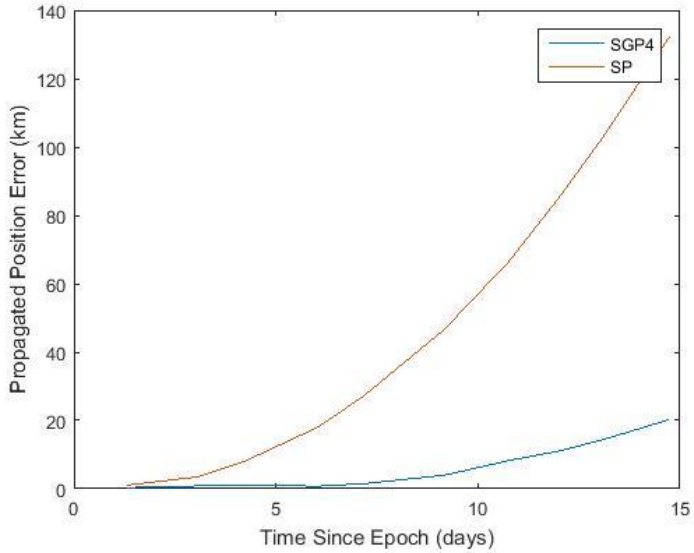

Figure 34: Test Case 18, SGP4 vs. Special Perturbations (2013 Data)

4.19 Test Case 19

Similar to the previous case, test case 19 showed an initially slow growth in the position error for Special Perturbations. However, again after the second day from epoch, the propagated position error increased rapidly. Meanwhile, the SGP4 positions remained closer to their predicted values.

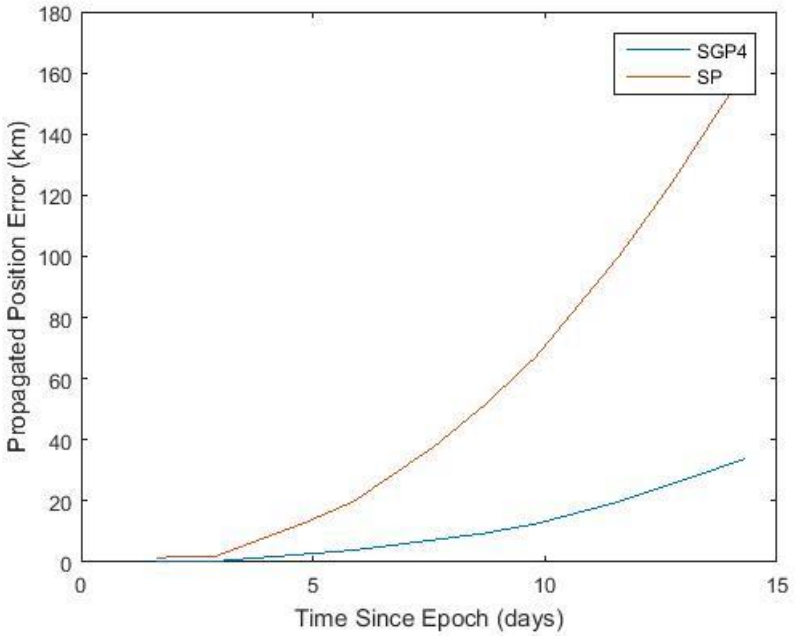

Figure 35: Test Case 19, SGP4 vs. Special Perturbations (2014 Data)

4.20 Test Case 20

Test case 20 involved the use of 2015 data. Figure 36 displays similar results, showing a larger starting error and rate of increase for the Special Perturbations model than for SGP4.

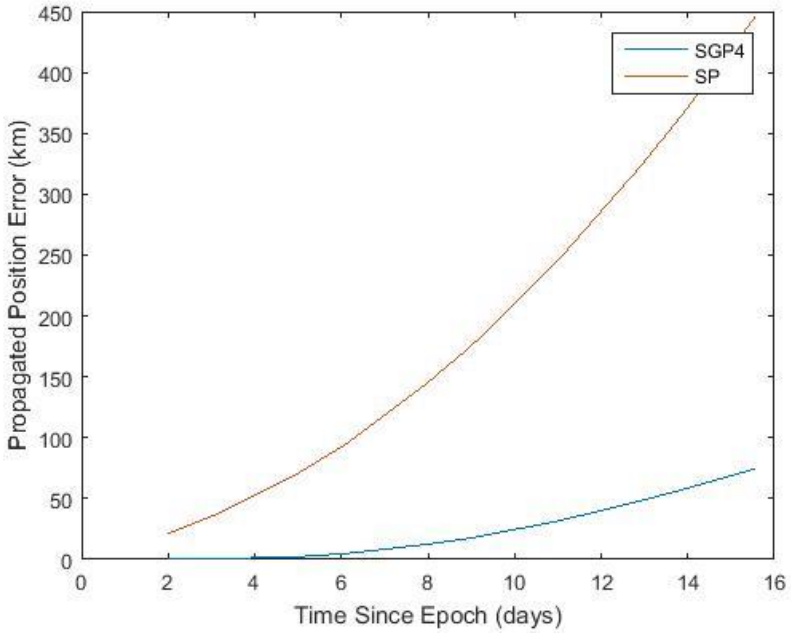

Figure 36: Test Case 20, SGP4 vs. Special Perturbations (2015 Data)

4.21 Test Case 21

In addition to the Hubble Space Telescope, four other objects were studied. Test case 21 focused on debris from a Delta IV launch vehicle. Two-line element sets were taken from 2009 for this object, starting with the first TLE of that year. With a perigee height of 580 km, this debris orbited slightly higher than Hubble. Both SGP4 and Special Perturbations models propagated the position error, as was done in the previous ten test cases. Figure 37 displays the results for the first ten element sets.

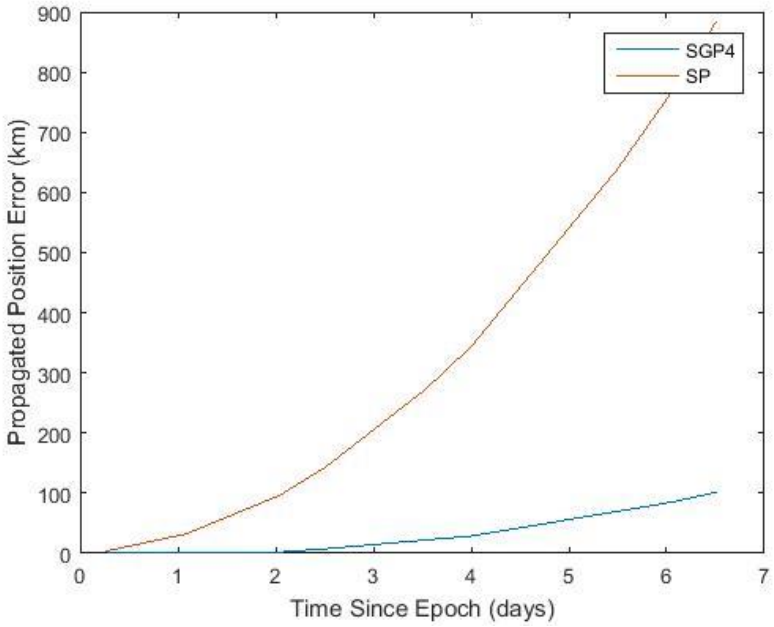

Figure 37: Test Case 21, Delta IV Debris Position Error (2009 Data)

As shown in the figure, the position error from the Special Perturbations model rapidly increases, surpassing 800 km by 6 days from epoch. SGP4, on the other hand, sees a large increase in the position error, although not even close to that of Special Perturbations.

4.22 Test Case 22

For test case 22, data was gathered on a rocket body from a Long March CZ-4B. Data was taken from element sets for the year 2016. This orbit had a perigee height of 562 km. Figure 38 displays the results. In this case, the Special Perturbations error grew quickly, though not as fast as the previous case. The error growth for SGP4 was erratic, and actually declined at some points. The propagated position for SGP4 remained quite close to the truth model though the first ten element sets.

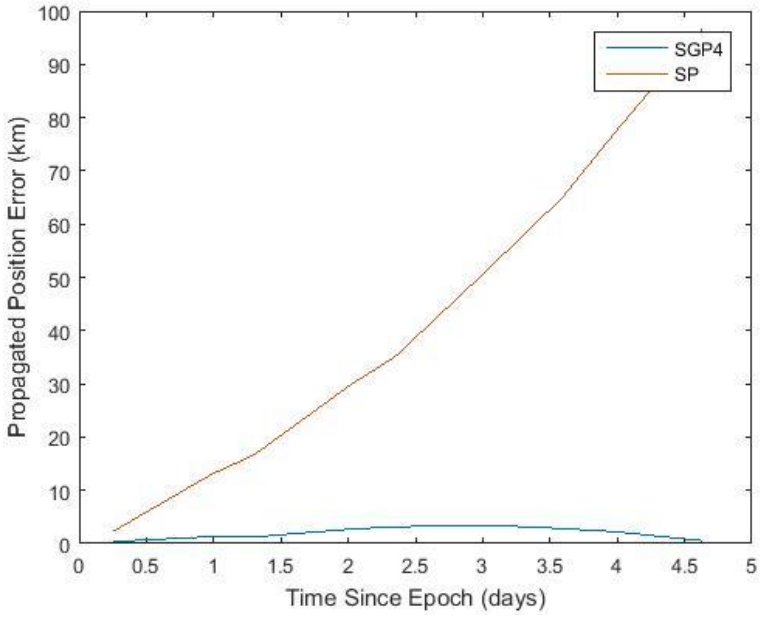

Figure 38: Test Case 22, CZ-4B Rocket Body Position Error (2016 Data)

4.23 Test Case 23

A rocket body from an Indian launched Polar Satellite Launch Vehicle was studied for test case 23, with TLE data taken from 2016. At that time, the perigee height was 420 km. As shown in Figure 39, the error growth from both models appear to increase in a quadratic fashion. However, the Special Perturbations model again quickly exceeds several hundred kilometers in the first few days from epoch.

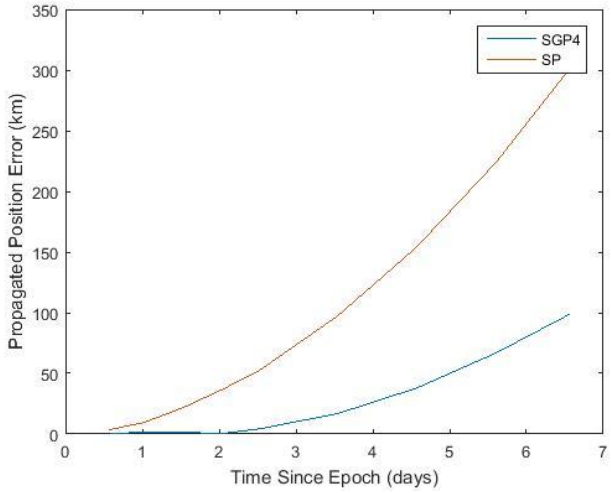

Figure 39: Test Case 23, PSLV Rocket Body Position Error (2016 Data)

4.24 Test Case 24

The final test case centered on a rocket body from a CZ-6 Long March launch vehicle. TLE data was taken from 2010. This rocket body orbited at a perigee height of 405 km, making it the lowest object studied. Figure 40 displays the results from the first ten element sets.

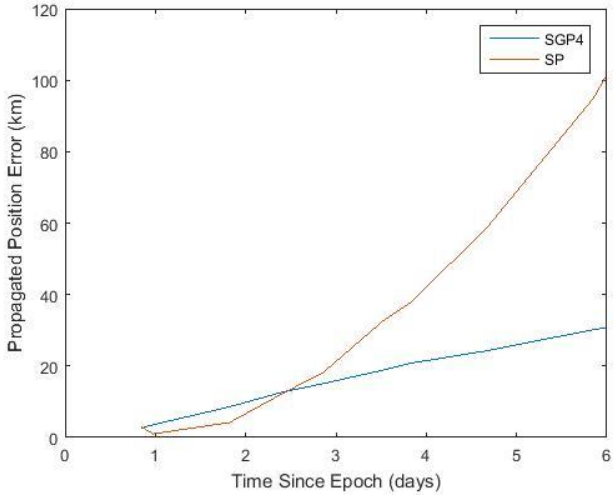

Figure 40: Test Case 24, CZ-6 Rocket Body Position Error (2010 Data)

Interestingly, the position error from Special Perturbations was actually lower than SGP4 for the first four element sets. After that point, however, the error from Special Perturbations rapidly grew, surpassing 100 km within 6 days from epoch.

As mentioned in Chapter III, the additional LEO objects provided for an opportunity to attempt to find a correlation between position accuracy and altitude. In order to compare the final four test cases with the Hubble Space Telescope, the data in Table 4 was averaged over all of the first ten test cases. Furthermore, the same process involving the average of 100 data points between element sets was implemented on the additional LEO objects. Thus, using only the SGP4 model, Table 4 displays the results in order of decreasing perigee height. Perigee height was chosen as the independent variable in this case, as the drag force on an object is maximized at perigee.

Table 4: Position Error Comparison

Object	Perigee Height (km)	Time Until 1 km Difference (Days)	Time Until 5 km Difference (Days)	Time Until 10 km Difference (Days)
Test Case 21	580	0.30	2.6	3.2
Test Case 22	562	1.4	5.8	6.1
HST	540	5.8	12.5	16.4
Test Case 23	417	1.0	2.0	2.7
Test Case 24	405	0.60	1.4	2.3

As shown in the data above, no definitive correlation was able to be made between perigee altitude and propagated position error. However, it should be noted that the object with the lowest altitude had the position error grow to 5 km and 10 km in the fastest time of all test cases. Furthermore, the Hubble Space Telescope displayed much better accuracy in the propagated position error than did any of the other objects.

4.25 Test Case 25

Test case 25 involved using the orbit fitting tool to obtain new initial position and velocity vectors for the Special Perturbations propagator. The TLEs used in test case 12 were also used for this test case. The initial element set was dated 6 January, 2010. The results are shown in Figure 41.

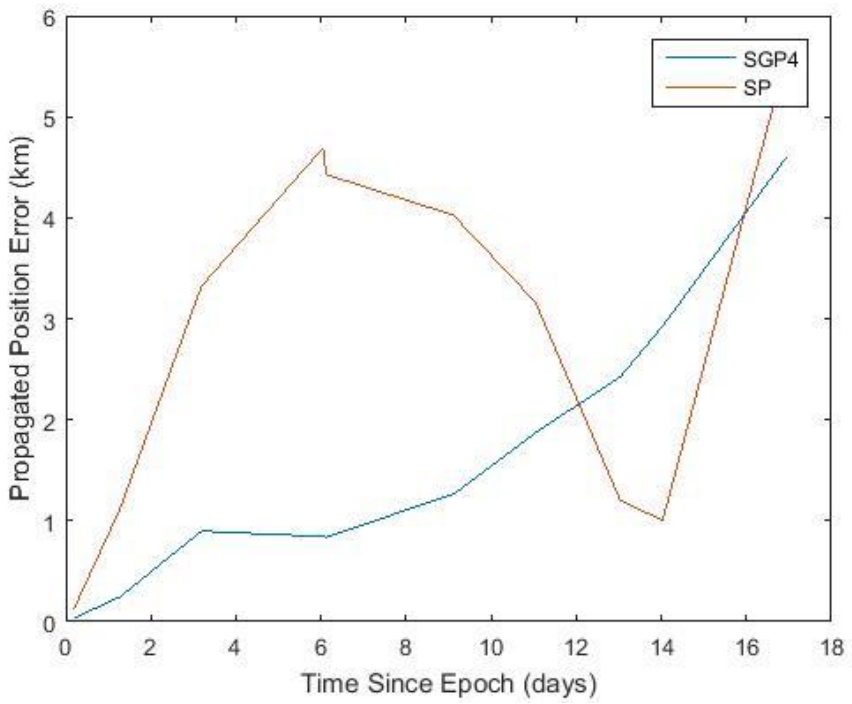

Figure 41: SGP4 vs. Special Perturbations (2010 data)

In comparison to test case 12, the Special Perturbations positions differed with the updated initial velocity vector. Although the behavior of the Special Perturbations model seems erratic, the propagated position growth does stay within 5 km for the first 15 days from epoch. This compares favorably to test case 12, where the position error was approaching 20 km during that same timeframe.

V. Analysis and Recommendations

This thesis strived to address the research questions posed in Chapter I, namely:

1. What orbit accuracy results can be obtained using TLEs as data with SGP4?
2. Similarly, what accuracy results can be obtained with TLEs using Special Perturbations as the orbit propagator?
3. For what period of time is a single TLE "good"?
4. Does TLE data contain information that can be better used by Special Perturbations?

In summary, the analytical model outperformed the numerical integrator in almost all of the test cases investigated. However, some element set comparisons resulted in a lower propagated position error for Special Perturbations than for SGP4 in the same time period.

5.1 Data Analysis

By referring to the first ten test cases, both the first and third research questions outlined were addressed. These test cases provided results on the consistency of SGP4 by computing the propagated position of an object from an initial element set and comparing it to future element sets. Additionally, Table 3 provides a convenient summary for this analysis. Using the Simplified General Perturbations 4 model, varying degrees of accuracy were obtained for the Hubble Space Telescope.

Based on the data procured, the results indicated that the propagated position remained within 1 km of the true position for a time period between 1.2 and 9.2 days. Similarly, the time period to exceed 5 km difference ranged from 4.1 to 22.7 days, while

the time to surpass 10 km position error was between 5.2 and 28.5 days. In an attempt to answer the third research question, a conclusion was drawn that after approximately 7 days from epoch, a single element set may no longer be able to predict the position of the object to within 1 km.

The wide variety of error growth charts indicate that each TLE has a large degree of uncertainty in the precision of its elements. Furthermore, taking data from years 2011 through 2015 for test cases 6 through 10 served two purposes: first, to generate a wide variety of initiating element sets; second, to attempt to find a correlation between error growth and the time at which the initial element set was taken.

Although the additional test cases did provide more diversity, no correlation could be made between year and propagated position error. Again referring to Table 3, the last five rows show no distinguishable pattern in the position error. In fact, the 2014 data showed the fastest error growth of the first ten test cases.

In order to address the second and fourth research question, data from test cases 11 through 25 must be analyzed. In almost every case, the error growth from the Special Perturbations model increased at a much higher rate than that of the SGP4 model. Overall, using the numerical propagator with the element set data produced poorer results. However, several data points (particularly in test cases 24 and 25) indicated a lower error using Special Perturbations for at least some of the TLE comparisons. Test case 25 indicated that better results were obtained using an orbit fitting tool to determine initial conditions for Special Perturbations.

5.2 Significance of Research

Overall, the results from the first ten test cases indicated a lower propagated position error with SGP4 than was found in previous studies. Furthermore, this thesis incorporated data from an entire year after the epoch of each of the initial element sets. The incorporation of this extended period of time allowed for a better understanding of how the propagated position error grows in a quadratic fashion with SGP4. Previous studies researched had only used data for a 15 day period from epoch.

Furthermore, using element sets as data was one of the most significant limitations of this research. As mentioned in Chapter II, *Spacetrack Report #3* states that the element sets produced by NORAD were computed with SGP4. Because of this, the TLEs used as data in this research were not intended for use with a numerical integrator. Therefore, a lower propagated position error with SGP4 than with Special Perturbations is an expected result while using TLEs as data.

The fact that several of the element set comparisons indicated a lower propagated position error with Special Perturbations than with SGP4 (particularly in test cases 24 and 25), therefore, is a promising result for the accuracy of the numerical integrator. The result is particularly promising because the numerical integrator outperformed the analytical model in these cases, even with the handicap of having to use the TLEs computed with SGP4 as data.

5.3 Recommendations for Future Work

Based on the data gathered, several recommendations are made. For a satellite operator, generating element sets as often as possible is desirable as it has been shown

that each TLE has a varying degree of uncertainty. Furthermore, having a smaller time period between element sets allows for an operator to have the most up to date information on the location of the satellite.

In regards to the research conducted, further improvements in both the analytical and numerical models should be made. As computing technology advances, numerical integration may provide an alternative option for element set computation and position propagation. The numerical integrator has the potential for higher order terms to be incorporated into the model. Also, if raw observation data is available, the use of it will provide a more accurate truth model and therefore more accurate comparisons between SGP4 and Special Perturbations. In summary, Special Perturbations provides for an opportunity for further research to be conducted.

5.4 Conclusion

Low Earth Orbit continues to be a congested environment. Accurately predicting satellite positions is vital for both military and civilian satellite operators and users. This thesis investigated an alternative method for satellite position prediction involving the use of the numerical integrator called Special Perturbations. Furthermore, the accuracy of two-line element sets was established using the Simplified General Perturbations model. The information provided in this thesis should lead to further research being conducted on alternative approaches to orbit estimation and two-line element set application. As more objects are launched into space, accurate satellite orbit predictions will become even more imperative.

Bibliography

[1] F. Cain, "How Many Satellites Are in Space?" *Universe Today*. http://www.universetoday.com/42198/how-many-satellites-in-space/, 2015.

[2] G. Levin, "Fifty Years Ago," *NASA Orbital Debris Quarterly News*, vol. 17, no. 3, pp-18, 2013.

[3] Elizabeth-Ann R. DeNeve, *Informing Spacecraft Maneuver Decisions to Reduce Probability of Collisions*, M.S. thesis, Department of Aeronautics and Astronautics, Air Force Institute of Technology, Dayton, OH, 2014.

[4] J. Liou, "Active Debris Removal," *NASA Orbital Debris Quarterly News*, vol. 15, no. 3, pp 7-8, 2011.

[5] D. J. Kessler, and B.G. Cour-Palais, "Collision Frequency of Artificial Satellites: The Creation of a Debris Belt," *Journal of Geophysical Research*, vol. 83, no. A6, pp 2637-2646, 1978.

[6] D. Vallado, *Fundamentals of Astrodynamics and Applications Fourth Edition*, Microcosm Press, Hawthorne, CA, 2013.

[7] W. Wiesel, "MyTruth" and "LeastSquares," C++ programs, 2016.

[8] D. Vallado, P. Crawford, R. Hujsak, and T.S. Kelso, "Revisiting Spacetrack Report #3," *AIAA*, vol. 6753, pp 1-88, 2006.

[9] F.R. Hoots, and R. L. Roehrich, "Spacetrack Report No. 3—Models for Propagation of NORAD Element Sets," *Spacetrack Report*, vol. 3, no. 3, pp 1-91, 1980.

[10] W. Wiesel, *Modern Orbit Determination 2nd Edition*. Aphelion Press, Beavercreek, OH, 2010.

[11] Systems Tool Kit, Analytical Graphics Incorporated, Version 10.0.0, 2012.

[12] G. Born, "Coordinate Systems," http://www.colorado.edu/ASEN/asen3200/handouts/Coordinate%20System.pdf, 2006.

[13] K. Dismukes, "Human Space Flight (HSF) - Realtime Data," *NASA*, http://spaceflight.nasa.gov/realdata/sightings/SSapplications/Post/JavaSSOP/orbit/ISS/SVPOST.html, 2011.

[14] T. S. Kelso "Orbit Determination," *Satellite Times*, vol. 1, no. 6, July/August 1995.

[15] T.S. Kelso, "Validation of SGP4 and IS-GPS-200D Against GPS Ephemerides," *17th American Astronautical Society/American Institute of Aeronautics and Astronautics Space Flight Mechanics Conference*, vol. 127, Part 1, pp 425-440, Sedona, AZ, 2007.

[16] W. Dong, and Z. Chang-yin, "An Accuracy Analysis of the SGP4/SDP4 Model," *Chinese Astronomy and Astrophysics*, vol. 34, no. 1, 2010.

[17] E. Kahr, O. Montenbruck, and K. O'Keefe, "Estimation and Analysis of Two-Line Elements for Small Satellites," *Journal of Spacecraft and Rockets*, vol. 50, no. 2, pp 433-439, 2013.

[18] W. Wiesel, *Modern Astrodynamics 2nd Edition*, Aphelion Press, Beavercreek, OH, 2010.

[19] Committee for the Assessment of the U.S. Air Force's Astrodynamic Standards, Aeronautics and Space Engineering Board, Division on Engineering and Physical Sciences, "Continuing Kepler's Quest – Assessing Air Force Space Command's Astrodynamics Standards," *National Research Council*, https://www.nap.edu/catalog/13456/continuing-keplers-quest-assessing-air-force-space-commands-astrodynamics-standards, 2012.

[20] A.B. Dunk, *Applying KAM Theory to Highly Eccentric Orbits*, M.S. thesis, Department of Aeronautics and Astronautics, Air Force Institute of Technology, Dayton, OH, 2014.

[21] C. Cao, W. Weinreb, and H. Xu, "Predicting Simultaneous Nadir Overpasses Among Polar-Orbiting Meteorological Satellites for the Intersatellite Calibration of Radiometers," *American Meteorological Society*, vol. 21, April 2004.

[22] M. Greene, and R. Zee, "Increasing the Accuracy of Orbital Position Information from NORAD SGP4 Using Intermittent GPS Readings," http://digitalcommons.usu.edu/smallsat/2009/all2009/65, 2009.

[23] O. Montenbruck, "Real-Time Estimation of SGP4 Orbital Elements from GPS Navigation Data," *International Symposium Spaceflight Dynamics*, Biarritz, France, 2000.

[24] T. Flohrer, H. Krag, and H. Klinkrad, "Assessment and Categorization of TLE Orbit Errors for the US SSN Catalogue," https://www.researchgate.net/publication/258327284_Assessment_and_Categorization_of_TLE_Orbit_Errors_for_the_US_SSN_Catalogue, 2008.

[25] T. S. Kelso, “Frequently Asked Questions: Two-Line Element Set Format,” *Satellite Times*, vol. 4, no. 3, January 1998.

[26] B.S. Lee, and J.W. Park, “Estimation of the SGP4 Drag Term from Two Osculating Orbit States,” *Journal of Astronomy and Space Sciences*, vol. 20, no. 1, 2003.

REPORT DOCUMENTATION PAGE

Form Approved
OMB No. 074-0188

1. REPORT DATE *(DD-MM-YYYY)*	2. REPORT TYPE	3. DATES COVERED *(From – To)*
23-03-2017	Master's Thesis	Aug 2015 – March 2017

TITLE AND SUBTITLE

Investigating Analytical and Numerical Methods to Predict Satellite Orbits Using Two-Line Element Sets

5a. CONTRACT NUMBER
5b. GRANT NUMBER
5c. PROGRAM ELEMENT NUMBER

AUTHOR(S)

Rich, Adam T. Captain, USAF

5d. PROJECT NUMBER
5e. TASK NUMBER
5f. WORK UNIT NUMBER

7. PERFORMING ORGANIZATION NAMES(S) AND ADDRESS(S)
Air Force Institute of Technology
Graduate School of Engineering and Management (AFIT/ENY)
2950 Hobson Way, Building 640
WPAFB OH 45433-8865

8. PERFORMING ORGANIZATION REPORT NUMBER
AFIT-ENY-MS-17-M-286

9. SPONSORING/MONITORING AGENCY NAME(S) AND ADDRESS(ES)

10. SPONSOR/MONITOR'S ACRONYM(S)
11. SPONSOR/MONITOR'S REPORT NUMBER(S)

12. DISTRIBUTION/AVAILABILITY STATEMENT
DISTRIBUTION STATEMENT A. APPROVED FOR PUBLIC RELEASE; DISTRIBUTION UNLIMITED

13. SUPPLEMENTARY NOTES

14. ABSTRACT

As Low Earth Orbit (LEO) contains an ever-increasing number of objects, the prediction of future object positions must be precise in order to avoid collisions. Object positions are distributed in two-line element (TLE) sets and are generated using the analytical propagator known as Simplified General Perturbations 4 (SGP4). However, a numerical integrator called Special Perturbations (SP) provides an alternative approach to TLE generation and propagation. In this thesis, TLE accuracy was determined with both models, and the length of time that a single element set can provide valid information was also established. With two-line element sets as data, comparisons were made between the numerical integrator and the analytical model for objects in LEO, particularly the Hubble Space Telescope (HST). The results obtained indicated that the propagated position error using SGP4 remained within 1 km of the expected position during a 7 day period from the epoch of the initial element set. Additionally, the majority of comparisons between SGP4 and SP resulted in a higher error while using the numerical integrator, although some comparisons showed a lower propagated position error with SP. This final result shows a potential for SP to provide more accurate position information than SGP4 in future research.

15. SUBJECT TERMS
Orbit estimation; Simplified General Perturbations; Special Perturbations

16. SECURITY CLASSIFICATION OF:			17. LIMITATION OF ABSTRACT	18. NUMBER OF PAGES	19a. NAME OF RESPONSIBLE PERSON
a. REPORT	b. ABSTRACT	c. THIS PAGE			William E. Wiesel, AFIT/ENY
U	U	U	UU	83	19b. TELEPHONE NUMBER *(Include area code)* (937) 255-3636 x4312

Standard Form 298 (Rev. 8-98)
Prescribed by ANSI Std. Z39-18